Atmos. Chem. Phys. Discuss., 14, 29237–29304, 2014
www.atmos-chem-phys-discuss.net/14/29237/2014/
doi:10.5194/acpd-14-29237-2014

Atmospheric Chemistry and Physics Discussions

Evaluating BC and NO_x emission inventories for the Paris region from MEGAPOLI aircraft measurements

H. Petetin[1,*], M. Beekmann[1], A. Colomb[1,2], H. A. C. Denier van der Gon[3], J.-C. Dupont[4], C. Honoré[5], V. Michoud[1,**], Y. Morille[4], O. Perrussel[5], A. Schwarzenboeck[2], J. Sciare[6], A. Wiedensohler[7], and Q. J. Zhang[1,*]**

[1]LISA/IPSL, Laboratoire Interuniversitaire des Systèmes Atmosphériques, UMR CNRS 7583, Université Paris Est Créteil (UPEC) et Université Paris Diderot (UPD), France
[2]Laboratoire de Météorologie Physique, Clermont-Ferrand, France
[3]TNO, Princetonlaan 6, 3584 CB Utrecht, the Netherlands
[4]Laboratoire de Météorologie Dynamique, Palaiseau, France
[5]AIRPARIF, Agence de surveillance de la qualité de l'air, Paris, France
[6]LSCE, Laboratoire des Sciences du Climat et de l'Environnement, CNRS-CEA-UVSQ, Gif-sur-Yvette, France
[7]Leibniz-Institute for Tropospheric Research, Leipzig, Germany
[*]now at: ARIA, Boulogne-Billancourt, France
[**]now at: Mines Douai, SAGE, Douai, France
[***]now at: Laboratoire d'Aérologie, Université Paul Sabatier and CNRS, Toulouse, France

Received: 6 May 2014 – Accepted: 30 October 2014 – Published: 24 November 2014

Correspondence to: H. Petetin (herve.petetin@lisa.u-pec.fr)

Published by Copernicus Publications on behalf of the European Geosciences Union.

ACPD
14, 29237–29304, 2014

Abstract

High uncertainties affect black carbon (BC) emissions and, despite its important impact on air pollution and climate, very few BC emissions evaluations are found in the literature. This paper presents a novel approach, based on airborne measurements across the Paris plume, developed in order to evaluate BC and NO_x emissions at the scale of a whole agglomeration. The methodology consists in integrating, for each transect, across the plume observed and simulated concentrations above background. This allows minimizing several error sources in the model (e.g. representativeness, chemistry, plume lateral dispersion). The procedure is applied with the CHIMERE chemistry-transport model to three inventories – the EMEP inventory, and the so-called TNO and TNO-MP inventories – over the month of July 2009. Various systematic uncertainty sources both in the model (e.g. boundary layer height, vertical mixing, deposition) and in observations (e.g. BC nature) are discussed and quantified, notably though sensitivity tests. A statistically significant (but moderate) overestimation is obtained on the TNO BC emissions and on EMEP and TNO-MP NO_x emissions, as well as on the BC/NO_x emission ratio in TNO-MP. The benefit of the airborne approach is discussed through a comparison with the BC/NO_x ratio at a ground site in Paris, which additionally suggests potential error compensations in the BC emissions spatial distribution over the agglomeration.

1 Introduction

Knowledge on pollutant emissions is a key element in the field of air pollution. It provides essential information on the contribution of various source sectors to pollutant levels, which is required for targeting emission reduction measures. Emission inventories are necessary input to chemistry-transport models (CTMs) which are important tools for atmospheric research and air quality management.

ACPD
14, 29237–29304, 2014

Among the various emitted species, black carbon (BC) aerosol is a chemical compound of major importance. In air quality, it highly contributes to the health risk (Peng et al., 2009) related to fine particulate matter ($PM_{2.5}$, particulate matter with aerodynamic diameter below 2.5 µm). It also plays a crucial role in the Earth's climate through the scattering and the absorption of incoming solar radiation and the subsequent change in planetary albedo (direct effect) (Schulz et al., 2006; Yu et al., 2006) and the modification of cloud properties as BC when coated with hydrophilic species acts as cloud condensation nuclei (indirect effect) (Lohmann and Feichter, 2005). The overall industrial era BC radiative forcing (including direct, semi-direct and indirect effects, as well as albedo change due to deposition on snow) is estimated at $+1.1\,W\,m^{-2}$, ranking second between the carbon dioxide (CO_2, $+1.56\,W\,m^{-2}$) and methane (CH_4, $+0.86\,W\,m^{-2}$) forcing (Bond et al., 2013).

However, high uncertainties still affect BC emission inventories making the true forcing per unit emitted uncertain. As a product of incomplete combustion processes, BC emissions at the global scale mainly originate from energy-related combustion (e.g. on- and off-road vehicles in transport area, biofuel and coal in residential area) and open burning (savannas and forest fires) (Bond et al., 2004, 2013; Junker and Liousse, 2008; Lamarque et al., 2010). Global BC emissions are most recently estimated at $7.5\,Tg\,year^{-1}$, with an uncertainty range of $2–29\,Tg\,year^{-1}$, of which $4.8\,Tg\,year^{-1}$ originate from energy-related combustion ($1.2–15\,Tg\,year^{-1}$) (Bond et al., 2013). Most values given in the literature are included in this large (factor 10) range. Granier et al. (2011) compared inventories over the past decades at different scales. In 2005, the ratio of the highest over the lowest global BC emissions estimate is only 1.28, but higher values are given at the regional scale in Western and Central Europe, with ratios of 1.34 and 1.76, respectively. Uncertainties arise from emission factors (usually highly dependent on the conditions of use and the type of equipment), activity data and spatial distribution for some source sectors (e.g. wood burning heating). By analysing a large number of source profiles, Chow et al. (2011) found highly variable BC contents in different $PM_{2.5}$ emission factors, in the range of 6–37 % for on-road light-duty gasoline

ACPD
14, 29237–29304, 2014

engine exhausts, 33–74 % for on-road heavy-duty diesel engine exhausts, 29–61 % for tire wear, 6–13 % for agricultural burning, 4–33 % for residential wood combustion and 3–14 % for oil combustion stationary sources. Dallmann and Harley (2010) have quantified uncertainties in $PM_{2.5}$ emission factors for various mobile sources, such as on-road gasoline (±45 %) and on-road diesel (±59 %) sources. On the contrary, the authors have estimated a much lower uncertainty in fuel consumption, around ±3 and ±5 % for on-road gasoline and diesel vehicles, respectively. In the evaluation of the BC climate impact, these uncertainties on emissions contribute – among other uncertainty sources such as microphysical interactions in clouds or removal processes – to a large 95 % confidence interval on the BC radiative forcing, between +0.17 and +2.1 $W m^{-2}$ (Bond et al., 2013). It is worthwhile noting that deducing local/regional scale BC emission uncertainties (for instance over the Paris megacity) from those at global scale, appears tricky. Indeed, if on the one hand uncertainties usually increase when considering smaller domains (because of uncertainties in spatial distribution of emissions), on the other hand some uncertainty sources relevant at global scale may be reduced at European scale (e.g. minor contribution of highly uncertain open burning emissions, better constrained local activity data). This is notably the case of a megacity like Paris located in a post-industrial country where the most uncertain sources have a low contribution.

Compared to BC, much more efforts have been made to assess NO_x emissions that in turn appear better constrained. In the inventories inter-comparison of Granier et al. (2011), the ratios between the highest and lowest NO_x emissions are 1.15 at global scale, and 1.18 and 1.23 in Western and Central Europe, respectively. Due to real-time measurements, large point sources emissions are expected to be reasonably estimated in countries with mandatory emission monitoring. Concerning the traffic source, which dominates the overall emissions (particularly in summer), uncertainties are still substantial. In bottom-up inventories, these emissions are usually estimated with traffic emission models of various types and complexities. Most uncertainties arise from both activity data and emission factors. Activity data are difficult to estimate as the

ACPD
14, 29237–29304, 2014

fleet and its technological characteristics (e.g. Euro standards) are perpetually evolving. Concerning emission factors, various techniques are available, both under controlled conditions or in real-world, and difficulties come up with their combination (see Franco et al., 2013 for a review). Compared to uncertainties previously given for $PM_{2.5}$ emission factors from Dallmann and Harley (2010), uncertainties for NO_x emission factors are significantly lower, with values around ±27 and ±22 % for on-road gasoline and on-road diesel sources, respectively. Smit et al. (2010) have reviewed results from 50 studies dealing with the validation of traffic emission models, and have pointed out a tendency to overestimate NO_x emissions whatever the validation techniques (e.g. tunnel, on-board or ambient concentration studies) or the model type (e.g. average-speed, traffic situation or modal model) employed. In their critical evaluation of on-road vehicle emission inventories over the United States, Parrish (2006) indicated rather accurate NO_x inventories in the 1990's but decreasing NO_x emission estimates during the last decade in contradiction with the tendency inferred from the evolution of NO_x concentrations. Additionally, in Monte-Carlo analysis where uncertainties on NO_x emissions are often considered, the two-sigma uncertainty ranges fixed for traffic NO_x emissions, usually taken from the literature and/or expert judgments, vary substantially in the literature: ±80 % (whatever the source) in Deguillaume et al. (2007) (deduced from the ±40 % one-sigma uncertainty given in the paper), ±100 % for area sources (and ±50 % for point sources) in Hanna et al. (2001) (also used in Tian et al., 2010), ±50 % for area sources (and ±3 % for point sources) in Napelenok et al. (2011).

The evaluation of these inventories still remains a critical point since emissions are generally not directly measurable. The use of CTMs for direct comparisons between measured and simulated concentrations is most of time inadequate to draw precise conclusions on emission inventories because concentrations measured at a receptor point cannot be unambiguously linked to emissions at a point aloft because of mixing processes and chemical transformations. In addition, CTMs and the meteorological input data they are using have their own uncertainties. Different alternative approaches have thus been developed. Concerning the BC emissions, useful information

ACPD
14, 29237–29304, 2014

may be gained from their evaluation relatively to those of another compound for which uncertainty in emissions is expected to be smaller. For example Zhou et al. (2009) derived BC emissions in two Chinese megacities from CO emissions and measured BC/CO ratios at sites 10–15 km downwind of the cities. However, given the large size of these megacities, the measurement representativeness for the city emissions remains an open question. Other methods specifically assess transport patterns of emissions to the receptor point. Xu et al. (2013) have developed a method based on in-situ measurements and backward trajectory analyses to evaluate BC emissions over the North China Plain. A promising approach consists in using inverse modeling techniques, which were widely applied to NO_x emissions using variationnal data assimilation (Mendoza-Dominguez and Russell, 2000), Bayesian Monte-Carlo approaches (Deguillaume et al., 2007; Konovalov et al., 2008), Kalman Filter approaches (Napelenok et al., 2008; Gilliland and Abbitt, 2001). NO_2 columns retrieved by satellites (e.g. form GOME, SCIAMACHY, OMI, GOME-2) provide a valuable observational basis for many of these works because of their large data coverage. For BC, the only study using variationnal data assimilation we are aware of is the one of Hakami et al. (2005) that aims at better constraining BC emissions over East Asia from in-situ measurements.

This paper presents an original methodology to evaluate emission inventories at the scale of a large city, based on airborne measurements in the city plume and chemistry-transport simulations. It is applied to BC and NO_x emission inventories over the Paris megacity, with the CHIMERE model. Observations used in this study were obtained in an intensive campaign that took place in and around the city in July 2009 in the framework of the MEGAPOLI European project (Megacity: emission, urban, regional and global atmospheric pollution and climate effect, and integrated tools for assessment and mitigation; www.megapoli.info). In particular, our study relies on airborne BC measurements in the city plume, trying thus to alleviate problems of representativeness of ground based in-situ measurements. In Sect. 2, the general methodology is described. All input data, including measurement data, emission inventories, and the CHIMERE model, are described in Sect. 3. Results from both ground and airborne

ACPD
14, 29237–29304, 2014

measurements are shown and discussed in terms of representativeness in Sect. 4. The various uncertainty sources are discussed in Sect. 5.

2 Methodology

The method developed in this study aims at evaluating, at the scale of a large city, emission inventories of species that can be traced at the scale of a few hours, i.e. either a chemically inert (at the time scale considered) single compound or a conservative family of products all originating from a unique primary compound. The method is based on airborne measurements of such species in the megacity plume during the afternoon in a well-mixed convective boundary layer (BL), so that the vertical mixing can be considered as rather well established, and consequently the measured concentrations at a particular altitude as representative of concentrations in the whole BL.

A CTM simulation, using the inventory to be evaluated, is used to simulate tracer concentrations in the plume. For both observations and simulations, along the flight path perpendicular to the plume, tracer concentrations above regional background and within the pollution plume can be integrated. The ratio of the simulated area over the measured area corresponds to a spatially averaged emission error factor (EEF) for the agglomeration for each flight. To achieve such a calculation, the plume needs to be well distinguishable from background, which requires large enough local emissions in the city and a rather homogeneous background.

This method aims at reducing the influence of some errors in the CTM. By considering integrated peak areas over lateral transects across the plume, it allows minimizing the effect of some potential errors in the structure of the simulated plume, e.g. any error on lateral dispersion, reasonable errors in wind direction, and consequently to focus more on emissions. However, several potential error sources still remain, and therefore need to be carefully investigated: (i) the wind speed which directly determines the temporal window of emissions sampled during the flight, (ii) the degree of vertical mixing which determines the representativeness of the airborne measured concentrations, (iii)

ACPD
14, 29237–29304, 2014

the wet and dry deposition of the tracer which can lead to discrepancies in the emissions factors if not well simulated by the model, and (iv) the boundary layer height and its horizontal variability over the aircraft trajectory which directly affects the level of concentrations. These points will all be discussed in the next sections.

The methodology is applied in this paper to BC and NO_x emissions. As a chemically inert compound, BC can be directly used as a tracer. For the NO_x compounds, as they undergo many fast chemical reactions, the NO_y family gathering all reactive nitrogen species (e.g. NO_x, NO_3, HNO_3, HONO, N_2O_5, PAN, ...) appears more conservative at the time scale of a plume, and is thus used as a tracer of NO_x emissions.

3 Input data

3.1 Measurement data base

In the framework of the EU FP7 MEGAPOLI project (Baklanov et al., 2010), two one-month intensive campaigns (July 2009 and January/February 2010) have been organized in the Greater Paris area to better characterize organic aerosol in a large megacity. The study presented here is based on observations obtained during the summer campaign.

Ground measurements of light absorption coefficient, elemental carbon (EC) and NO_x have been performed Paris at the LHVP (*Laboratoire d'Hygiène de la Ville de Paris*) station (48.829° N, 2.359° E) (urban background site in the center of Paris). The light absorption coefficient (at a measured wavelength of 637 nm, different from the instrument nominal wavelength of 670 nm) is measured by a Multi-Angle Absorption Photometer (MAAP) at a 5 min resolution. EC concentrations are provided by an OCEC Sunset Field instrument at a resolution of one hour. NO_x observations come from a chemiluminescence monitor equipped with molybdenum oxide converters. However, an efficient conversion of many other nitrogen-containing compounds ($NO_z = NO_y - NO_x$) by the molybdenum converter can lead to interferences in the NO_x

ACPD
14, 29237–29304, 2014

concentrations (Dunlea et al., 2007). This positive artefact varies from one location to the other, depending on the relative contribution of NO_z compounds in the NO_y family. Dunlea et al. (2007) have estimated a mean overestimation of +22 % in Mexico City.

Among the chemical data available in the Paris plume, NO_y and BC airborne measurements aboard the French ATR-42 aircraft have been used (see Freney et al., 2013, for a detailed description of the aircraft campaign). Measurements are available for several days in July: 1, 9, 10, 13, 15 (only BC that day), 16, 20 (only NO_y), 21, 25, 28 (only BC), 29 (only NO_y). NO_y concentrations were measured at a 30 s time resolution with an instrument designed for airborne measurements that consists of three Ecophysics analyzers in which NO is measured using ozone chemiluminescence. NO_2 is photolytically converted, and NO_y is converted with H_2 in a gold covered heated oven (see Freney et al., 2013, for details). The limit of detection is 10 pptv. NO, NO_2 and NO_y measurement uncertainties have been estimated by these latter authors to 10, 20 and 20 %, respectively. The measured NO_y includes the following species: NO, NO_2, HNO_2, HNO_3, HO_2NO_2, N_2O_5, PAN, PPN and particulate nitrate. BC particles are collected with a 50 % passing efficiency aerodynamic diameter of 5.0 µm (McNaughton et al., 2007), but most soot particles are likely in the fine mode. The light absorption coefficient is measured with a 60 s time resolution from the light absorption coefficient at 650 nm provided with a Particle Soot/Absorption Photometer (PSAP) instrument, corrected as in Bond et al. (1999) (see Supplement, Sect. S1, for details). PSAP absorption coefficient measurement uncertainties are around 20–30 % (Bond et al., 1999; Virkkula et al., 2005). Absorption values are then converted into BC concentrations using a mass-specific absorption coefficient (MAC) of 8.8 $m^2\,g^{-1}$ derived from a linear regression between MAAP and OCEC Sunset measurements at the LHVP site (R^2 = 0.88, N = 533, see Sect. S2 in the Supplement, for details). This MAC is also used to derive BC concentrations from the MAAP observations at the LHVP site. The uncertainty related to the MAC is discussed in Sect. 5.4.

Various physical parameters are also measured in the ATR-42 aircraft at a 1 s time resolution including wind speed, wind direction and position of the aircraft (longitude,

ACPD
14, 29237–29304, 2014

latitude, height). BL height (BLH) estimations are available at the SIRTA (*Site Instrumental de Recherche par Télédétection Atmosphérique*) (48.712° N, 2.208° E) (sub-urban background site at about 20 km in south-west of Paris) and LHVP stations. At SIRTA, they are estimated from ALS450 Leosphere backscatter lidar data at a 5 min time resolution (Haeffelin et al., 2012). At LHVP, values are estimated from CL31 ceilometer data (Haeffelin et al., 2012). Traditional meteorological parameters (wind, temperature) are also measured at SIRTA where, additionally, Leosphere wind cube lidar measurements are also available, providing wind measurements at a 10 min time resolution, each 20 m from 40 to 200 m above ground level (a.g.l.).

3.2 Emission inventories

Three European anthropogenic emission inventories are evaluated in this paper, all referring to year 2005:

1. The EMEP inventory (Vestreng et al., 2007).

2. An inventory developed partly in the framework of MEGAPOLI project by TNO. The inventory for the year 2005 was constructed using official emissions submitted by European countries (downloaded from EEA in 2009) in combination with a gap-filling procedure using IIASA RAINS or TNO default data. The compiled emission data were spatially distributed at a resolution of $1/8^\circ \times 1/16^\circ$ longitude–latitude (approximately 7 km × 7 km). The development of the gridded data is described in Denier van der Gon et al. (2010) and Pouliot et al. (2012). It is the year 2005 base case inventory and also serves as a starting point for the inventory described next. In this paper it is referred to as the TNO inventory.

3. A third inventory based on the TNO inventory but incorporating bottom-up emission data over the four European megacities (Paris, London, Rhine-Ruhr and Po valley). The city emission inventories were compiled by local authorities responsible for city emissions inventories and air quality such as Airparif for Paris (Airparif,

ACPD
14, 29237–29304, 2014

2010). It is described in more detail by Denier van der Gon et al. (2011), and has been previously used in Zhang et al. (2013) and Timmermans et al. (2013). It will be referred as the TNO-MP (MP for MegaPoli) inventory.

The same EC/OC speciation table, primarily associated to the TNO inventory, is applied in all inventories. Sector-dependent factors used to derive July emissions from annual ones are reported in Table S1 in the Supplement. This table also shows the total sectorwise BC July emissions over the region for the three inventories.

The resolution of both TNO and TNO-MP inventories is considerably improved compared to the EMEP inventory whose resolution is $0.5^\circ \times 0.5^\circ$. Despite its coarse spatial resolution, the comparison of this latter inventory with the two other refined ones remains relevant for several reasons: (i) before being applied to simulations, emissions are downscaled to the air quality model resolution, here to a 3 km horizontal resolution, using the 1 km × 1 km-resolved GLCF (Global Land Cover Facility) landuse database (Hansen et al., 2000; Hansen and Reed, 2000), and (ii) concentrations are considered in the Paris plume, i.e. at a rather large spatial scale, which decreases the influence of such a coarse resolution in the emissions. Emissions are apportioned according to several types of landuse: urban, rural, forest, crops and maritime (Menut et al., 2013). Because of their better horizontal resolution, the evaluation of emission inventories in this paper focused mainly on the TNO and the TNO-MP inventories, the EMEP is taken as an additional reference emission inventory, as it is used in many studies in Europe.

The spatial distribution of BC and NO_x emissions in the Paris region during a typical working day in July is given in Fig. 1 for each inventory. In order to illustrate the important differences in the spatial distribution of emissions between inventories, one can compute for all inventories the mean emissions of all cells within a certain distance around the LHVP site, from 0 (only the LHVP cell) to 80 km (the whole region). This is shown in Fig. 2 for all inventories relatively to the TNO-MP one.

Relatively to TNO-MP, the EMEP inventory BC and NO_x emissions in the Paris center are relatively low, but increase further away. The coarse resolution and the effect of the previously mentioned emission downscaling are clearly visible for EMEP emissions,

ACPD
14, 29237–29304, 2014

and lead to obvious discontinuities between original cells. At a large scale, it gives the highest emissions for both compounds (and more particularly for NO_x emissions). Conversely, TNO and TNO-MP inventories display significantly higher emissions in the agglomeration center, and lower ones further away. In summer, the TNO-MP inventory shows a quite similar spatial emission distribution as the TNO one. In particular, major highways around Paris, spatially unresolved or missing in the EMEP inventory, are clearly visible thanks to the refined resolution. However, BC emissions in TNO-MP are considerably lower than in TNO in the agglomeration. In absolute terms, discrepancies between both inventories mainly originate from road transport (SNAP sector 7) and residential/tertiary (SNAP 2) sources, and in a lesser extent from waste disposal (SNAP 9), non-road transport (SNAP 8) and industrial process (SNAP 4) sources (see Table S1 in the Supplement for details). However, the highest relative discrepancies (that exceed a factor of 3) are associated to SNAP 2, 8 and 9. For sources considered as area in the top-down TNO inventory (e.g. SNAP 2 and 9), they are likely due to the distribution proxies used to downscale national totals, leading to too high emissions in Paris where the population density is very strong (Denier van der Gon et al., 2010). Concerning the SNAP 4 point sources, discrepancies can probably be explained by the use of generic capacity rules in TNO, rather than exact emissions in the TNO-MP. Both inventories are equivalent outside this region. A quite similar pattern is given for NO_x emissions, except that discrepancies between both inventories in Paris are much reduced. In terms of BC/NO_x emission ratios, highest values are given by the TNO inventory, followed by the EMEP one, and finally the TNO-MP one. Differences are maximum in the center of Paris, and decrease when integrating over larger areas.

3.3 CHIMERE model description

In this paper, all simulations are performed with the CHIMERE CTM (Schmidt et al., 2001; Bessagnet et al., 2009; Menut et al., 2013) (www.lmd.polytechnique.fr/chimere). The model was originally designed to provide (i) short-term predictions of ozone and aerosol concentrations and (ii) long-term (several years) predictions asso-

ACPD
14, 29237–29304, 2014

ciated to emissions control scenarios. Besides research activities, it allows operational air quality survey and forecasting, and is used by different local air quality agencies in France (AASQA) and abroad, and by the French organization INERIS for daily air quality forecasting in France and Europe (PREVAIR service, www.prevair.org). At European scale, it is also used within the Copernicus GMES-MACC program.

The CHIMERE model allows simulating transport, gas-phase chemistry, some aqueous-phase reactions, size dependent aerosol species including secondary organic aerosol (SOA), dry and wet deposition. It treats coagulation, absorption as well as nucleation aerosol processes. Inorganic aerosol thermodynamic equilibrium is calculated using the ISORROPIA model (Nenes et al., 1998).

3.4 Model configuration and simulated cases

In this paper, simulations are performed during the summer MEGAPOLI campaign (July 2009) with a five-day spin-up period. As shown in Fig. 3, two nested domains of increasing resolution (CONT3 and MEG3) are considered, their characteristics being reported in Table 1. The choice of the domains was previously explained in Zhang et al. (2013). The domain is subdivided into eight vertical layers, from ground to more than 5000 m height, with vertical resolution decreasing with altitude. The first three layers have a depth of about 40, 70 and 110 m, respectively.

Boundary and initial conditions are taken from LMDz-INCA2 global model for gaseous species and LMDz-AERO for particulate species (Hauglustaine et al., 2004; Folberth et al., 2006). The model uses the previously described anthropogenic emission inventories, while biogenic emissions are computed with MEGAN data and parametrizations from Guenther et al. (2006). In order to investigate the influence of meteorology on results, two meteorological dataset are considered. The first has been produced with PSU/NCAR Mesoscale Meteorological model (MM5; Dudhia et al., 1993), performed over three nested domains with increasing resolutions of 45, 15 and 5 km respectively, and using Global Forecast System (GFS) data from the National Center for Environmental Prediction (NCEP) as boundary conditions and large scale

ACPD
14, 29237–29304, 2014

data. The second one has been produced with the Weather Research and Forecasting model (WRF; Skamarock et al., 2005; wrf-model.org) for the same domains and resolutions.

3.5 Black carbon/elemental carbon terminology

Petzold et al. (2013) have recently made some recommendations about the use of the term "BC" for black carbon, distinguishing various terminologies depending on the property used in the measurement technique: (i) the light absorbing coefficient σ_{ap}, or equivalent BC (EBC) if the MAC is indicated, for instruments based on light absorption, (ii) refractory BC (rBC) for instruments based on refractory properties, (iii) elemental carbon (EC) for instruments focusing on the chemical composition or the carbon content based on thermo-optical methods.

So far in this paper, the term BC has been employed as a qualitative and commonly used terminology. As both PSAP and MAAP instruments are based on the measurement of the light absorption, observations should thus be referred as EBC. However, as emission factors and source profiles used to build emission inventories are mostly expressed as EC (Vignati et al., 2010; Chow et al., 2011; H. A. C. Denier van der Gon, personnal communication, 2011), the simulated "BC" should be regarded as EC. An ambiguity therefore arises from comparisons between observed EBC and modeled EC since they correspond to different quantities. This point is discussed in Sect. S2 in the Supplement and in Sect. 5.4. In the following, the term BC will be kept for convenience for both observations and simulations.

4 Results and discussion

In this section, we first evaluate meteorological input data. A simple approach is then applied to evaluate BC emissions against NO_x ones, based on ground based measurements at the urban background LHVP site in Paris. We then describe the proce-

ACPD
14, 29237–29304, 2014

dure to evaluate BC emissions based on airborne measurements in the Paris plume, and present the corresponding results. We finally discuss discrepancies between both methods.

Statistical metrics are defined as:

$$\text{Mean bias: MB} = \frac{1}{n}\sum_{i=1}^{n}(m_i - o_i) \quad (1)$$

$$\text{Normalized mean bias: NMB} = \frac{1}{n}\sum_{i=1}^{n}\frac{(m_i - o_i)}{\overline{o}} \quad (2)$$

$$\text{Root mean square error: RMSE} = \sqrt{\frac{1}{n}\sum_{i=1}^{n}(m_i - o_i)^2} \quad (3)$$

$$\text{Normalized root mean square error: NRMSE} = \frac{1}{\overline{o}}\sqrt{\frac{1}{n}\sum_{i=1}^{n}(m_i - o_i)^2} \quad (4)$$

$$\text{Correlation coefficient: } R = \frac{\sum_{i=1}^{n}(m_i - \overline{m})(o_i - \overline{o})}{\sqrt{\sum_{i=1}^{n}(m_i - \overline{m})^2 \sum_{i=1}^{n}(o_i - \overline{o})^2}} \quad (5)$$

Where m_i and o_i are the modeled and observed concentrations at time i, respectively, and $\overline{m}$ and $\overline{o}$ their averages over the period.

4.1 Evaluation of meteorological data

4.1.1 Ground observations

In this section are investigated the meteorological input data used in CHIMERE simulations, with both MM5 and WRF models. The Fig. 4 shows comparisons between observations and simulations for meteorological parameters obtained at the SIRTA ground

ACPD
14, 29237–29304, 2014

site. Statistical results are reported in the Table 2, considering all hours as well as only the 06:00–14:00 UTC time period (designed hereafter as morning hours), more relevant in our methodology since transport from the urban emission sources to the aircraft location occurs in the morning and the early afternoon.

Except the first days of a continental north-easterly wind regime, the period is dominated by an oceanic regime with west and south-west winds. The MM5 model shows a negative bias of −0.87 °C for ground temperature (reduced to −0.45 °C by considering only morning hours), and a positive one on wind speed (+33 %). BLH appears strongly underestimated, with a bias of −34 %, reduced to −24 % during morning hours. Satisfactory correlations are found for temperature (due to diurnal cycle) and wind speed (R around 0.8–0.9), but lower ones are obtained for BLH (around 0.5). Conversely, the WRF model shows better results on temperature (now slightly overestimated, with a bias of +0.45 °C) and overall BLH with an underestimation reduced to −17 % (and −12 % during morning hours). Correlations on this latter parameter are significantly improved compared to MM5 model (0.7 against 0.5).

As one of the factors contributing to the BLH negative bias, diurnal profile comparisons on Fig. 5 show that the transition from a convective to a stable BL in the evening hours occurs much too early in the MM5 model, particularly at the LHVP site. This shift carries on with WRF but is seriously reduced, which explains the better correlations.

4.1.2 Observations in altitude

Wind lidar observations are compared with simulated wind speed in the first model layers (the first vertical layers in CHIMERE are at 43, 118 and 248 m a.g.l.) (see Fig. S3 in the Supplement). Due to a low vertical resolution in simulations, comparisons remain qualitative. MM5 and WRF models show quite similar patterns, but the MM5 model tends to give a higher wind speed at all levels, including at ground. Statistical results over the 06:00–14:00 UTC time window in the 110–210 m altitude range and for the flight days are reported on Table 3. In average, low negative biases and reasonable NRMSE are obtained with both MM5 and WRF models. At the daily scale, biases on

ACPD
14, 29237–29304, 2014

wind speed remain below ±30 %, except the 13, 16 and 28 July (respectively the 29 July) during which one or both models give high underestimations (respectively overestimation), up to −46 % (respectively +27 % with MM5). Errors in terms of NRMSE exceed 25 % for all these dates, as well as during the 21 July (above 26 %) despite a low bias (error compensation between an underestimation during the first hours and overestimation during the last hours).

Wind speed simulation results are much better along the aircraft path (not shown), all biases remaining below ±20 % while NRMSE range between 12–32 %. The highest biases occur the 1 and 28 July, around −18 %. From a general point of view, the moderate positive bias found on wind speed at ground vanishes in altitude except at mid-altitude during specific days, leading to a noticeable decrease of the NRMSE.

4.2 Emission corrections from ground measurements

BC emissions can be first evaluated relatively to those of NO_x, by assuming that both concentrations are proportional to their emissions close to their sources. Urban background BC and NO_x concentrations, their ratio and their diurnal profiles are presented in Fig. 6. Statistical results are reported in Table 4. In order to be comparable with the airborne approach, only flight days are considered, but some results over the whole month of July will also be indicated.

Observed BC displays a characteristic diurnal profile with a main peak during the morning rush hours, and a more progressive increase at the end of the day. Hourly concentrations range between 0.1–5.7 $\mu g\,m^{-3}$, with a 1.0 $\mu g\,m^{-3}$ mean concentration. Highest BC concentrations are observed on 1, 16, 28 and 29 July, due to low wind speed conditions, at least in the morning (below $\sim 1\,m\,s^{-1}$ at ground, Fig. 4). Background levels are particularly high on 1 July due to both a clear north-east origin of air masses and a low wind speed, that have allowed a slow and intense BC accumulation in air masses over Northern France, Belgium and the Netherlands before reaching Paris. CHIMERE simulations with MM5 data show an overestimation above a factor of 2 whatever the inventory, particularly during morning and evening BL transitions.

ACPD
14, 29237–29304, 2014

Largest biases occur with the TNO inventory (NMB of +260 %). The meteorology has a significant influence, as shown by the much lower biases obtained with WRF data during evening BL transitions, due to improvements in BLH simulation. In particular, since primary pollutants are highly sensitive to BL dynamics, these improvements lead to significant increase of correlations, approximately from 0.4 to 0.7. Underestimated nighttime BLH with both meteorological models, sometimes associated to low wind speed, is likely to explain some highly overestimated peaks (e.g. 16 July).

Measurements give a mean NO_x concentration around 22 ppb, with values reaching up to 141 ppb. As expected due to common emission sources with BC, NO_x compounds show very similar variations, as do model biases. Again, simulations with WRF meteorology give lower concentrations than MM5 ones, leading to reduced but still positive biases for all inventories except EMEP that underestimates NO_x concentrations. As for BC, both correlation and NRMSE are significantly improved with WRF prediction.

Observed BC/NO_x ratios remain rather constant over the period, around $0.06\,\mu g\,m^{-3}\,ppb^{-1}$ in average. They appear more variable during the night maybe due to higher spatial heterogeneities induced by the lower wind speed and the nocturnal boundary layer stability. In particular, very high peaks observed on 20 and 25 July (up to $0.3\,\mu g\,m^{-3}\,ppb^{-1}$) may be related to specific unidentified local BC pollution events in the shallow boundary layer while NO_x concentrations are very low. The diurnal profile shows minimum values during the early morning, and a significant increase at the end of the day in observations, due to previously mentioned peaks. Also simulations show rather constant BC/NO_x ratios along the day, without any clear diurnal pattern. Ratios are significantly overestimated by the TNO inventory (NMB of +131 %) and to a much lesser extent by the EMEP inventory (+67 %), while a low bias is obtained with the TNO-MP inventory (+13 %). The influence of dynamics is mostly removed, as attested by the quite similar results with both MM5 and WRF meteorological data. All these discrepancies between inventories are consistent with the discussion in Sect. 3.2 (Fig. 2).

ACPD
14, 29237–29304, 2014

It is worthwhile noting that, even if both BC and NO_x are mainly locally emitted within the Paris agglomeration, biases may be partly related to errors in advected contributions: BC can be transported from outside (like on 1 July), while some NO_x may be advected during the night and the early morning (when its photolytic conversion into HNO_3 or HONO is not active) or released by reservoir species (e.g. PAN). NO_x measurements at two rural background stations in the south and south-east of Paris are available from the AIRPARIF network. In average, the NO_x regional background roughly accounts for 15–25 % and 15–30 % of the levels in Paris for observations and simulations, respectively. From one year measurements during the PARTICULES campaign (Bressi et al., 2013), it has been found that the BC regional background contributes to about a third to the annual BC urban background average in Paris, and that this fraction is probably underestimated by the CHIMERE model (Petetin et al., 2013). However, this uncertainty source remains difficult to quantify more precisely. Additionally, NO_x chemiluminescence measurements may also include some NO_z compounds (Dunlea et al., 2007), but this is not likely a large error source since the CHIMERE model gives an average NO_x/NO_y ratio above 92 % at the LHVP site.

Given all these elements, we thus consider the BC/NO_x ratio over the 05:00–8:00 UTC time window, corresponding to rush hours where fresh NO_x and BC are expected to dominate. BC vs. NO_x concentrations during that time window are represented in Fig. 7. Results reported in Table 5 show a high overestimation for the TNO inventory, around a factor of 4. Overestimations are reduced to a factor of 2.8 and 2.2 for EMEP and TNO-MP inventories, respectively. Uncertainties on emission error factors (at a 95 % confidence interval) are quite the same for all inventories, around 18 %, since they essentially originate from the uncertainty on the slope deduced from observations (i.e. BC/NO_x ratios are more variable in observations than in simulations). Note also that discrepancies between BC vs. NO_x slopes and BC/NO_x ratios (whose biases remain below +136 %) are due to the diurnal variability of the measured BC/NO_x ratio that shows the lowest values during the 05:00–08:00 UTC time window.

ACPD
14, 29237–29304, 2014

Results finally indicate an overestimation of BC emissions relative to NO_x emissions, particularly in both top-down inventories (EMEP and TNO), that is significantly reduced with local bottom-up information integrated in the TNO-MP inventory.

4.3 Airborne evaluation of BC and NO_x emissions

Given these first results obtained at ground, the alternative approach based on airborne measurements in the plume is now presented. The procedure is first described in details, and the results are then shown.

4.3.1 Procedure to compute emission error factors (EEF)

As an illustration, the TNO/MM5 case as well as two flights on the 10 and 13 July are considered. Aircraft trajectories and BC concentrations during these days are presented in Fig. 8 (time series for all July flights are given in Fig. S4 in the Supplement). As previously mentioned, the inlet used to collect BC particles is characterized by a 50 % passing efficiency aerodynamic diameter of 5.0 µm, and BC measurements are thus compared to the simulated BC concentration below 5 µm. Time series given in Fig. 9 show a series of peaks that correspond to successive crossings of the plume. In both observations and simulations, the Paris region plume is well distinguishable against background, and peaks can thus be located on the trajectory, giving the approximate central line of the plume. Errors in the simulated wind direction lead to a shift in the spatial localization of the plume (e.g. 13 July). It is worthwhile noting that some plumes from other cities may sometimes be sampled by the aircraft. The case of the 13 July is notable: slight increases in BC concentrations in the western part of the flight track (after 13:00 UTC) correspond to plumes from Rouen and Le Havre, two industrial cities.

Concentration variations at the end of the flight correspond to a vertical profile up to 3 km a.g.l. performed by the aircraft. We focus in this study on the time period during which the aircraft altitude is rather constant (about 600 m a.g.l.). As briefly described

ACPD
14, 29237–29304, 2014

in Sect. 2, the methodology consists in computing for each transect the plume integral of concentrations above background, this latter being estimated in both model and observations as the 30 percentile of concentrations in one transect (Fig. 10). Only points above the background value are taken into account, and additionally, some adjustments are made when winds bring plumes from other cities close to the Paris one.

Given that the aircraft does not exactly cross the plume perpendicularly, but with an angle α between 0 and 90° that may be different in simulations compared to real world, a correction factor of $\sin(\alpha)$ is thus computed and applied to each peak area. Considering that atmospheric diffusion theories predict a linear relationship between point source emissions and concentrations in the plume, an emission error factor is finally defined for each flight as the ratio of the simulated area over the observed one (i.e. an error factor of two means an emission overestimation of 100 %).

The emission error factor is finally defined as:

$$\mathrm{EEF}_{\mathrm{flight}} = \frac{\sum_{\mathrm{peak}} \sin(\alpha_{\mathrm{mod,\,peak}}) \int_{\mathrm{peak}} (C_{\mathrm{mod}}(t) - C_{\mathrm{mod,\,background}}) \mathrm{d}t}{\sum_{\mathrm{peak}} \sin(\alpha_{\mathrm{obs,\,peak}}) \int_{\mathrm{peak}} (C_{\mathrm{obs}}(t) - C_{\mathrm{obs,\,background}}) \mathrm{d}t} \quad (6)$$

It is worthwhile noting that such an evaluation applies to the combination of: (i) the PM emission inventory, (ii) the PM speciation into BC, (iii) the monthly emission factor for July and (iv) the hourly emission profile. If uncertainties are expected to be larger on the two first elements, the two others may also contribute to the errors. In the following discussion, it is to be kept in mind that the reference to BC emissions aggregates all these elements.

ACPD
14, 29237–29304, 2014

4.3.2 BC and NO_x emission error factors

BC and NO_x emission error factors are given for each flight on Fig. 11. Average results and confidence intervals are also reported, considering errors as multiplicative:

$$\text{Mean: } \overline{\text{EEF}} = \exp\left(\frac{1}{n}\sum_{\text{flight}=1}^{\text{nflights}} \ln(\text{EEF}_{\text{flight}})\right) \quad (7)$$

Confidence interval on the mean:

$$\sigma_{\overline{\text{EEF}}} = \exp\left(\frac{2}{\sqrt{n}}\sqrt{\frac{1}{n}\sum_{\text{flight}=1}^{\text{nflights}} (\ln(\text{EEF}_{\text{flight}}) - \ln(\overline{\text{EEF}}))^2}\right) \quad (8)$$

Mean BC emissions results are quite contrasting between inventories and suggest in average a slight overestimation of the EMEP inventory (+9 % with MM5 data), a large overestimation of the TNO inventory (+45 %) and an underestimation of the TNO-MP inventory (−18 %). Results on NO_x inventories show an overestimation ranging between +29 and +39 % depending on the inventory. As previously mentioned, NO_y measurements may include a part of nitrate aerosols, but including them in the model has a very slight influence on results (NO_x mean error factor changes remain below 11 % for all inventories). Despite some discrepancies on specific days between MM5 and WRF results, both give rather similar average emission biases. However, due to the strong variability from one day to the other, uncertainties on these average values are high for all inventories and both species, with a factor of about 1.39–1.47 for MM5 cases (at a 95 % confidence interval) but reduced to 1.27–1.31 for WRF simulations.

Such a high day-to-day variability was not expected, which raises the question of its origin: does it come from the real-world emissions (missing in the model emission input data), or is it induced by uncertainties in the methodology, or both? In the following subsections, the variability potentially associated to observations themselves is dis-

ACPD
14, 29237–29304, 2014

cussed, while the variability that may come from the methodology (e.g. model errors) will be investigated in Sect. 5.

4.3.3 BC/NO_x emission factors ratio

In order to characterize this variability, one can first investigate ratios of BC emission error factors over NO_x ones. If BC and NO_x sources are colocalised and show a similar time evolution, then taking the BC/NO_x ratio should allow normalizing out errors related to simulated transport, and consequently reduce the variability. Ratios are given on Fig. 12, and statistical results are reported in Table 6.

BC/NO_x average ratios appear underestimated in EMEP and TNO-MP inventories (−18 and −46 %, respectively), while a very low EEF (+7 %) is found for the TNO inventory. However, the day-to-day variability remains as high as that of BC and NO_x taken individually, with an uncertainty on the mean around a factor 1.31–1.41. In particular, rather small BC/NO_x error factor ratios are obtained the 1, 13 and 21 July (and the 25 with MM5 meteorology), compared to the other days. However, the model underestimation on these particular days is due to a higher observed BC/NO_y ratio not captured by the model, as shown by the calculations of the BC area over NO_y area performed for observations and simulations separately (Fig. S5 in Supplement). Observed ratios on these days are above 0.15 close to a factor of two higher than values obtained the other days (around 0.06–0.09). And yet, the model fails to reproduce such an enhancement, which explains results obtained in Fig. 12.

The reasons for such an increase are not clear. On 1 July, BC measurements around Paris (and notably upwind of the city) show rather high but noisy concentrations (see Fig. S6 in Supplement), which suggests a possible heterogeneity in the BC regional background. In our methodology, a unique regional background value is estimated, based on the whole flight. In the case of a rather slender BC plume coming from the north in the axis of the Paris and adding itself to the city plume, our procedure would thus not be able to discriminate both. This may explain the high BC/NO_y ratio observed on that day.

ACPD
14, 29237–29304, 2014

4.3.4 Time window of emission sampling

Another possible source of variability in the BC/NO_x emissions is related to the time window of emission sampling. The Paris plume sampled by the plane in the early afternoon at a distance up to 100 km from the city center originates from prior emissions, over different time windows depending on the wind speed. Practically, during a day with strong wind speed (typically more than 5 m s^{-1}), the earliest emissions may be already advected too far away (and diluted too much) to be sampled by the aircraft. Such a situation often occurs, as visually confirmed by non-zero last sampled peak during most flights (see Fig. S4 in Supplement). And conversely, in case of low enough wind speed, pollutants emitted during night may be still in the plume during the afternoon.

In order to assess which emissions are sampled in each flight, a new simulation case is run with the MM5 meteorology during the July month with 16 tracer compounds emitted each hour in a cell in the center of Paris, from 00:00 to 16:00 UTC. These inert compounds are only advected and deposited on the ground. By interpolating their concentration along each flight path, it is possible to compute the contribution of emissions at a specific hour to the overall plume. The Fig. 13 gives an illustration for 28 July, for which wind speed at higher levels is among the lowest (3.8 m s^{-1}, see Table 3). Tracer emissions follow a working day emission profile. Early morning emissions of the day (in cold colors) dominate the two last peaks, while the latter emissions contribution (in green and hot colors) progressively increases in earlier peaks. The contribution of emissions at a specific hour is given by the integral ratio of the associated tracer concentration over the total concentration (black area on the figure). On this flight, the aircraft thus sample emissions over a quite large time window (00:00–11:00 UTC), with main contributions originating from 05:00–07:00 UTC emissions (that account for 50 % of the total area).

The procedure is repeated for each flight, and contribution results for all flights are presented on Fig. 14, colored according to their average wind speed in altitude (Table 3). Due to the large daily wind speed variability, sampling is quite different from

ACPD
14, 29237–29304, 2014

one flight to the other. Largest windows (00:00–11:00 UTC) are sampled during the 13, 16 and 28 July flights, for which wind speed remains quite low. Most of other flights (1, 9, 10, 20, 25 July) with intermediate wind speed have a sample window around 06:00–11:00 UTC, while the strongest wind speeds occurring the 15 and 21 July lead to sampling of 09:00–12:00 UTC emissions.

As BC/NO_x emission ratios do not have a constant diurnal profile, ratios in the plume are also expected to vary from one day to the other, depending on the wind speed. In particular, the average BC/NO_x diurnal profile observed at the LHVP site (Fig. S7 in the Supplement) shows lower values during morning rush hours than in the end of the morning (~ 0.05 against $\sim 0.07\,\mu g\,m^{-3}\,ppb^{-1}$). As only late emissions are sampled on 21 July, this may explain higher ratios obtained in the plume. Unfortunately, no NO_y measurements are available the 15 July with similar high wind speeds to confirm such a tendency. However, that explanation as well as the one previously given for the 1 July does not apply to the 13 July flight for which the high ratio thus remains unexplained.

4.4 Representativeness issues

Results obtained at ground in Paris show an overestimation of both BC and NO_x concentrations. As this may be due to uncertainties in the simulation of meteorology (e.g. boundary layer height), no quantitative assessment can be made on both individual emission inventories, while for the case of the BC/NO_x ratio the influence of meteorological variables is reduced. Results finally suggest an overestimation of this ratio in the TNO inventory, and at a lesser extent in the EMEP one, while quite correct values are given by TNO-MP. This is not consistent with results obtained for the plume where the BC/NO_x emission ratio appears underestimated in all inventories, in particular in the TNO-MP one.

Several reasons may at least partly explain these discrepancies between ground and airborne results. The main one is probably the difference of representativeness between both approaches, ground concentrations being influenced by emissions in the vicinity of the LHVP station, while concentrations in the plume integrate emissions at

ACPD
14, 29237–29304, 2014

a much larger scale (the whole agglomeration). In order to assess the LHVP site representativeness, a simulation with traced emissions around that site is performed over a few days (see Sect. S.2 in the Supplement). LHVP concentrations appear mainly influenced by close emissions, with a contribution of 50–85 % from emissions within a radius of 6 km around the site. Conversely, beyond a radius of 21 km (which still covers the agglomeration), emissions contribute to less than 10 %. These contributions are quite variable depending on the wind field, the importance of close emissions increasing with stagnant conditions. Since BC and NO_x emissions as well as their ratio are highly heterogeneous over the whole Paris region (Sect. 3.2), results obtained at the LHVP site thus cannot be representative for the whole agglomeration, but probably only for its central part.

Additionally, the previous tracer experiment takes into account neither the sub-grid emissions heterogeneity at a resolution of 3 km × 3 km (e.g. a park and a stretch of the Paris ring are included in the LHVP cell) nor sub-cell processes, caused by the high complexity of urban environments (e.g. street canyons, building-induced turbulence). The LHVP spatial representativeness may thus be even lower. Working at the plume scale strongly reduces these limitations since (i) all emissions within the agglomeration end up in the plume, and (ii) mixing during a few hours of transport from the source regions to the measurement locations is expected to significantly increase the concentration representativeness.

This would therefore suggest that the best BC/NO_x emission ratio is given by the TNO-MP inventory in the Paris center, while it highly underestimates the ratio at the scale of the whole agglomeration, contrary to the TNO inventory which gives better results. Compared to TNO-MP, NO_x emissions in that last inventory are quite similar while BC ones are higher and more concentrated in the center of Paris.

However, these discrepancies may also partly arise from several uncertainty sources at stake in our methodology, that are discussed in the next section.

ACPD
14, 29237–29304, 2014

5 Uncertainties of the inversion methodology

The methodology used to evaluate NO_x and BC emission inventories based on aircraft data over the Paris region intends to minimize several error sources: (i) the representativeness error by considering concentrations in the plume rather than at ground, (ii) modeled chemistry errors by considering inert tracer species/families, and (iii) lateral dispersion and plume direction errors by considering integrated concentrations. The high emission error factors day-to-day variability previously noticed is partly due to a variability in Paris agglomeration emissions, but such large discrepancies are not expected, and are indicative of other uncertainty sources that must be at stake, among which: (i) the wind field errors and their impact on emissions really sampled by the plane, (ii) BLH height errors and vertical mixing, (iii) errors in deposition, and finally (iv) discrepancies between EBC and EC. All these uncertainty sources are investigated in this section. Overall emission error factors uncertainties are discussed in Sect. 5.5.

5.1 Wind speed and emission profiles

As previously mentioned in Sect. 4.3.4, the methodology does not evaluate emissions alone but also a part of the applied diurnal emission profiles. Potential errors on wind speed may shift the time window, over which emissions are sampled (in simulations with respect to reality). This causes an additional uncertainty all the more important that the time window is narrow and temporal emission gradients are important. In addition, wind speed errors within the city directly determine the residence time of air masses close to emission sources and thus the degree of pollutant accumulation.

Significant wind speed NRMSE at the SIRTA site, both at ground and at altitude levels below 200 m a.g.l. (around 40–60 and 10–60 %, respectively), have been found (Sect. 4.1). These errors influence the accumulation of emitted pollutants within the city, for which uncertainties are thus probably quite important, as the accumulation time is at first order inversely proportional to the wind speed. Thus, this uncertainty in the local wind speed appears as an important source of uncertainty and variability

ACPD
14, 29237–29304, 2014

in the day to day emission error factors. On the contrary, biases in the wind speed are reasonable, for example mostly below ±30 % for the wind speed at SIRTA between 100 and 200 m a.g.l., thus indicating no particular bias in emission error factors due to this error source.

Another uncertainty source is related to wind speed errors at higher altitudes (between the agglomeration and the measurement location), and subsequent errors on the plume advection. Given the diurnal profile of emissions and the variable emission time window sampled by the plane depending on the wind speed (Sect. 4.3.4), an error on advection would shift that time window toward earlier (respectively later) emissions in case of negative (respectively positive) biases on wind speed in altitude. This error source thus appears all the more important that the gradient in the diurnal profile sampled part is high. Daily biases on wind speed below ±20 % have been found in airborne measurements along the flight path. If these uncertainties are taken as representative for the average wind between the emission source and the aircraft, the typical displacements of the emission time window are less than about 1 h. This would induce significant errors (say above 10 %) only for time windows between 03:00 and 06:00 UTC, when the temporal gradient in emissions is strong. Thus this error source should not be of major importance to explain the variability in results.

5.2 Vertical mixing and boundary layer

As previously highlighted, compared to urban background heterogeneities (expected to be important due to the proximity of sources), considering aircraft measurements in the plume rather than observations at ground gives a better representativeness of emission corrections. However, this is based on the assumptions that (i) the vertical mixing in the BL is correctly established, so that observations obtained in the plane, at an altitude of about 600 m a.g.l., can be considered as representative of those in the whole plume, and (ii) the model correctly retrieves the BLH and the vertical mixing within.

ACPD
14, 29237–29304, 2014

5.2.1 Boundary layer height

The BLH is the first important parameter that requires to be correctly modeled, since it determines the volume into which the emissions will be diluted within the plume. During early afternoon, Lidar observations at SIRTA and LHVP sites have shown an underestimation by MM5 model, while significant improvements are obtained with WRF model but still with a negative bias at the SIRTA suburban site (Sect. 4.1.1). If such an underestimation exists in the whole flight region, it may lead to an overestimation of emission biases. However, processes are not linear, since the increased concentrations due to a lower BLH may for instance be reduced by a higher dry deposition (that depends on concentrations in lowest level). In order to assess the importance of these errors, a sensitivity test is performed with the EMEP/MM5 case by increasing the BLH by 30 % (corresponding to the mean bias between 06:00–14:00 UTC). So far, simulated cases have been performed with prognostic turbulent parameters (i.e. directly taken from meteorological models). However, as the diffusivity coefficient depends on the BLH, the sensitivity test with BLH multiplied by 130 % is performed with the diagnostic option, in which the vertical turbulent diffusivity coefficient (K_z) is calculated within the CTM among others as a function of the PBL. Relative changes on emission error factors are presented on Fig. 15. Except for some specific dates (10, 20 and 28 July), a larger BLH leads to lower concentrations and therefore decreases error factors. On average, changes are around −14 % for both BC and NO_x, and have rather no influence on the mean BC/NO_x ratio (−1 %). Thus, the uncertainty in PBL heights could both contribute to the variability and bias in BC and NO_x emission error factors, while the BC/NO_x ratio is rather unaffected by these errors.

5.2.2 Vertical mixing

Besides the BLH, another important aspect is the vertical mixing within the boundary layer, and the ability of the CHIMERE model to catch the vertical distribution of pollutants. The highest vertical heterogeneity of primary pollutants concentration is

ACPD
14, 29237–29304, 2014

expected above the city, due to emissions mostly located at surface, while vertical gradients are expected to decrease gradually along the plume due to the turbulent mixing and the absence (or the relatively poor contribution) of fresh emissions at ground outside the city. In our methodology, the aircraft measurement representativeness indeed relies on the assumption that the vertical mixing is already established for the first transect across the plume, or at least that incomplete vertical mixing is correctly simulated. The vertical turbulent mixing parametrization in the CHIMERE model follows the K-diffusion approach of Troen and Mahrt (1986) without counter-gradient term. Vertical fluxes are directly proportional to K_z that is bounded in the model by a minimum value of 0.01 and 1 $m^2 s^{-1}$ in the dry and cloudy BL, respectively, and by a maximum value of 500 $m^2 s^{-1}$ (Menut et al., 2013). To assess the influence of vertical mixing on results, a sensitivity test is performed by multiplying and dividing K_z values by two, as in Vautard et al. (2003). Both the dry minimum and the maximum boundaries are kept in the sensitivity test. Relative changes are shown in Fig. 15.

Dividing (respectively multiplying) the K_z by two leads to a moderate increase below +19 % (respectively a decrease below −16 %) for BC and NO_x, while the BC/NO_x ratio does not change by more than 6 %. Such small changes are quite consistent with the results obtained over the Paris agglomeration by Vautard et al. (2003) who explain the moderate impact of K_z on concentrations in altitude by the fact that a larger diffusivity increases both the incoming vertical flux from lower layers and the outgoing one toward higher layers.

5.3 Deposition

BC and NO_y are expected to be conservative at the time scale of the flight, but they both undergo deposition. Errors in the simulated deposition and/or in the NO_y speciation (given the large differences of deposition rates among NO_y individual compounds) may impact emission biases results. Meteorological conditions indicate that wet removal is likely to be negligible over the campaign region, and the deposition is thus essentially dry. In order to assess the influence of deposition on results, a sensitivity test based on

ACPD
14, 29237–29304, 2014

the EMEP/MM5 case is performed without any dry or wet deposition. Relative changes on BC, NO_x error factors and on their ratios are reported on Fig. S8 in the Supplement. Removing deposition increases all error factors by various amounts depending on the day. On average, error factor changes on BC and NO_x are around +7 and +16 %, respectively. Without deposition, the BC/NO_x error factor ratio is decreased by −9 % in average. These figures are upper limits, as errors in deposition speed are most probably less than 100 %. Thus, uncertainty in deposition likely does not very much affect the error budget.

5.4 Mass-specific absorption coefficient (MAC)

As previously mentioned in Sect. 3.5, an additional uncertainty may arise from the comparison between EBC (observations) and EC (emissions and simulations), through the MAC value used to convert absorption coefficients into EBC concentrations. Airborne PSAP EBC concentrations have been obtained considering a constant MAC of $8.8\,m^2\,g^{-1}$ deduced from measurements at the LHVP site in Paris (see Sect. S2 in the Supplement). The relevancy of comparisons performed in this study with the simulated EC thus relies on the hypothesis that this MAC determined in the Paris center is valid at the scale of the whole agglomeration, and that it remains constant along the flight. This is supported by the MAC value estimated in winter 2009 by Sciare et al. (2011) at a suburban site at 20 km in the south-west of Paris that remains in the same order of magnitude than the one obtained here in the Paris center ($7.3 \pm 0.1\,m^2\,g^{-1}$). Actually, during that winter season, but one year later, single particle Aerosol Time-Of-Flight Mass Spectrometer observations performed at the LHVP site during the MEGAPOLI winter campaign have shown a majority of already internally mixed BC particles (with a shell of organic material and secondary inorganic compounds) (Healy et al., 2012). Therefore, the MAC variations along the flight are expected to be reasonable. This is also supported by the analysis of BC/NO_y ratios obtained from aircraft observations that does not show any significant increase with distance from Paris, which would be expected if the MAC value increased with distance from the emission source. Addi-

ACPD
14, 29237–29304, 2014

tionally, it is worthwhile noting that direct measurements of the MAC enhancement by Cappa et al. (2012) have recently shown a very low enhancement between near source and more distant values, only by around +6 %, onboard a ship along the California coast (CalNex campaign) and at a ground site located at 14 km of Sacramento (Carbonaceous Aerosols and Radiative Effects Study, CARES campaign). Considering the previous MAC estimations in the Paris region – 7.3 and 12.0 by Sciare et al. (2011) and Liousse et al. (1993), respectively – the uncertainty associated to our MAC value is roughly estimated at 30 %.

5.5 Overall discussion

Results obtained for each compound in Sect. 4.3 consist in mean error factors and rather large confidence intervals that result from (i) uncertainties associated to the day-to-day variability which is not included in the model input data (beyond the temporal dependence on the month and the day of the week), (ii) measurement uncertainties and (iii) uncertainties in the methodology (conditioned by error sources in the model).

The first ones are difficult to quantify but can reasonably be considered as random. Also measurement uncertainties are probably mostly random, but may include a part of systematic uncertainties. In order to be conservative, they are assumed entirely as systematic. Uncertainties in the methodology have been discussed in previous sections, notably through various sensitivity tests on deposition, boundary layer height and the turbulence diffusivity coefficient. Results have shown that all investigated uncertainties in the model influence mean emission error factors, and their variability. They have therefore a systematic and a random part, which we could estimate in the previous sensitivity tests. These tests have shown a significant day-to-day variability, which suggests that they are probably partly random and may thus explain most of the day-to-day variability obtained in first results (in Sect 4.3). It appears rather tricky (and uncertain) to explain all discrepancies between individual flight results on a quantitative basis, notably due to the fact that several uncertainty sources are potentially combined. In spite of that, the choice is made to replace the uncertainty obtained in Sect. 4 by a combi-

ACPD
14, 29237–29304, 2014

nation of all the uncertainties estimated in this section. Results of individual and the derived overall systematic uncertainty are reported in Table 7.

Confidence intervals on average emission error biases deduced from the overall uncertainty are reported in Table 8. For NO_x emissions, positive biases are found in all inventories. Considering the 95 % confidence intervals, the bias in the TNO inventory appears statistically insignificant, which may not be the case in both EMEP and TNO-MP inventories for which a slight overestimation remains probable (due to a confidence interval lower bound of −4 %, thus very close to zero). These are in the range of the 35 % agreement found for NO_x emissions in Paris during the ESQUIF project in summer 1999 by Vautard et al. (2003) also based on airborne measurements and CHIMERE simulations, but using an alternative method, and an older emission inventory prepared by AIRPARIF. Through an inverse modeling exercise based on satellite NO_2 columns, Konovalov et al. (2006) have obtained a similar 30 % overestimation of the EMEP inventory in the Paris area. Through another inverse emission modeling based on ground measurements over the Paris region, Deguillaume et al. (2007) have found no significative bias, but an uncertainty of about ±20 %. Note that these studies were performed using different emission inventories. Given the uncertainties, the NO_x emissions positive bias around 20–30 % found here in most of the inventories does not appear as significant.

Also both the positive bias (around +12 %) of EMEP and the negative one (around −23 %) of TNO-MP BC emissions are not significant, while the 95 % confidence interval of the TNO inventory indicates a probable overestimation of BC emissions in that inventory. As previously mentioned in Sect. 3.2, the overestimation of BC emissions in the TNO inventory can probably be explained by the spatial distribution procedure that concentrates too large emissions in the city. For example, using population density as a proxy implies the assumption of constant per capita emissions over the country which might lead to an overestimation of urban BC emissions as discussed in Timmermans et al. (2013) and references therein. At this stage, it is to be emphasized that discrepancies between EMEP and TNO BC results are mostly related to differences in

ACPD
14, 29237–29304, 2014

their spatial resolution since input data for national totals are similar. Accordingly, Paris region total emission in July are quite similar in both EMEP and TNO inventories (as shown in Table S1 in Supplement). However, at the scale of the Paris agglomeration, total emissions in both inventories do show discrepancies, TNO emissions being more concentrated in the city due to its finer resolution while the EMEP emissions spill over in rural areas of Paris region due to their coarser resolution (see Sect. 3.2). Therefore, to our sense, the better results obtained with EMEP have to be interpreted with caution. Potential errors in the distribution of BC emissions are partly avoided in the TNO-MP inventory which follows a more (but not fully) bottom-up approach. Concerning the BC/NO_x emission ratio, the only statistically significant negative bias concerns the TNO-MP inventory, while results for both EMEP and TNO inventories suggest an error compensation in BC and NO_x emissions, leading to a satisfactory estimation of BC/NO_x emission ratio. It is worthwhile reminding that, in this study, the same BC speciation table (primarily built for the TNO inventory) has been used in all inventories in order to be consistent, but the use of a more specific speciation to the Paris region would maybe change these results, in particular for the TNO-MP inventory in which a part of the bottom-up information is lost through the use of a constant BC speciation in this study. Another point to be mentioned concerns the emissions interannual variability that adds an additional uncertainty (similar for all inventories) due to the comparison of observations from 2009 with inventories built for 2005.

To our knowledge, a BC emissions evaluation as presented here has not yet been attempted at the scale of a large megacity, and uncertainties estimated at the global or regional scale are difficult to extrapolate to an agglomeration. For comparison, through their adjoint inverse modeling exercise over Asia, Hakami et al. (2005) have found quite consistent total assimilated and base case BC emissions over Asia, but have underlined higher discrepancies at regional scale, with major errors over Japan, northern and southern China of about a factor 2.

ACPD
14, 29237–29304, 2014

6 Conclusion

Black carbon (BC) emissions are still highly uncertain, and very few studies have attempted to evaluate their inventories. This paper presents an original approach, based on airborne measurement across the Paris plume, developed in order to evaluate BC and NO_x emissions at the scale of the whole agglomeration. Basically, the method consists in integrating over each transect observed and simulated concentrations above background. Such an approach aims at minimizing various error sources in the model: (i) representativeness errors by considering airborne measurements in the plume rather than observations at ground, (ii) chemistry errors by considering inert compounds (BC) or conservative families (NO_y as a tracer of NO_x emissions), (iii) lateral dispersion and plume direction related errors by integrating concentrations rather than performing strict pair-wise comparisons. The methodology is applied to the evaluation of three inventories with the CHIMERE chemistry transport model: the EMEP inventory, and the so-called TNO and TNO-MP inventories, constructed in the framework of the MEGAPOLI project, the last one including bottom-up refined data from the local air pollution agency AIRPARIF over the Paris region.

In order to assess the benefit of such a methodology, BC/NO_x ratios at the LHVP ground site in Paris are first investigated. Over the whole July month, they show a significant (at a 95 % confidence interval) overestimation in all inventories with biases ranging between a factor of 2 in TNO-MP and a factor of 4 in TNO. However, these results are judged as representative only for an area surrounding the LVHP site in a few kilometers of distance. On average, results obtained from July airborne observations give an overestimation of NO_x emissions around +20–30 % for all inventories, a moderate bias around +12 and −23 % for EMEP and TNO-MP BC emissions, respectively, but a higher positive bias of +40 % for TNO BC inventory. However, these results present an unexpected high day-to-day variability (up to a factor of about 3). Low biases are also obtained on BC/NO_x emission ratio for EMEP and TNO invento-

ACPD
14, 29237–29304, 2014

ries (−18 and +13 %, respectively), contrary to the TNO-MP inventory that shows an underestimation of −44 %.

Various uncertainty sources in the methodology are investigated through sensitivity tests – wind field errors, boundary layer height, vertical mixing, deposition, BC nature (equivalent BC vs. elemental carbon) – and are likely to explain this variability. Results of these tests are used to derive a systematic uncertainty between 35 and 48 % on emission error factors. This suggests that a moderate overestimation of NO_x July emissions in EMEP and TNO-MP inventories is statistically probable. Biases found in EMEP and TNO-MP BC emissions are not significant. However, the overestimation in TNO BC emissions does appear as significant, probably due to the distribution proxies used to downscale national total emissions that concentrate too large emissions in a highly populated area such as Paris with lower per capita emissions. The BC/NO_x emission ratio appears underestimated in the TNO-MP inventory, while non significant biases are obtained with both EMEP and TNO inventories. While discrepancies between EMEP and TNO inventories are likely due to differences in spatial resolutions and allocation, the ones between TNO and TNO-MP do illustrate the distinction between bottom-up and top-down approaches.

At the end, best estimations of BC and NO_x emission biases thus do not exceed ±40 %, which appears as rather moderate considering the numerous uncertainties at stake in the construction of an inventory. Due to methodological uncertainties in the same order of magnitude, assessing the significance of all these results remains difficult. However, the methodology does succeed in highlighting some statistically significant biases, and in particular, whether on BC and NO_x emissions or on the BC/NO_x ratio, at least one of the three inventories has been proven as very probably biased. It is worthwhile noting that the methodology used in this study not only evaluates an inventory by itself but also a particulate matter speciation table and a temporal disaggregation (monthly and diurnal) that are also subject to potential errors.

To our knowledge, this study is one of the most comprehensive ones to evaluate BC emissions at the scale of a large megacity. The comparison of aircraft- and ground-

ACPD
14, 29237–29304, 2014

based results has given an interesting insight on the potential error compensation in the spatial allocation of BC emissions over a large agglomeration. In the framework of the PRIMEQUAL PREQUALIF project, a dense BC network of 14 stations (of various typologies, e.g. rural, urban, traffic) has been installed over the Paris region. It will allow a better characterization of the BC spatial distribution over the agglomeration, and in the line of this, an interesting outlook would thus be to compare it to the simulated spatial distribution constrained by emission inventories.

The Supplement related to this article is available online at doi:10.5194/acpd-14-29237-2014-supplement.

Acknowledgements. The research leading to these results has received funding from the European Union's Seventh Framework Programme FP/2007-2011 under grant agreement no. 212520. The authors also acknowledge the ANR through the MEGAPOLI PARIS and INSU/LEFE through the MEGAPOLI France project for their financial support. This work is funded by a Ph.D. DIM (*domaine d'intérêt majeur*) grant from the Ile-de-France region.

References

Airparif: Inventaire des émissions en Ile-de-France, Méthodologie et résultats année 2005, 2010 (in French).

Baklanov, A., Lawrence, M., Pandis, S., Mahura, A., Finardi, S., Moussiopoulos, N., Beekmann, M., Laj, P., Gomes, L., Jaffrezo, J.-L., Borbon, A., Coll, I., Gros, V., Sciare, J., Kukkonen, J., Galmarini, S., Giorgi, F., Grimmond, S., Esau, I., Stohl, A., Denby, B., Wagner, T., Butler, T., Baltensperger, U., Builtjes, P., van den Hout, D., van der Gon, H. D., Collins, B., Schluenzen, H., Kulmala, M., Zilitinkevich, S., Sokhi, R., Friedrich, R., Theloke, J., Kummer, U., Jalkinen, L., Halenka, T., Wiedensholer, A., Pyle, J., and Rossow, W. B.: MEGAPOLI: concept of multi-scale modelling of megacity impact on air quality and climate, Adv. Sci. Res., 4, 115–120, doi:10.5194/asr-4-115-2010, 2010. st

ACPD
14, 29237–29304, 2014

Bessagnet, B., Menut, L., Curci, G., Hodzic, A., Guillaume, B., Liousse, C., Moukhtar, S., Pun, B., Seigneur, C., and Schulz, M.: Regional modeling of carbonaceous aerosols over Europe – focus on secondary organic aerosols, J. Atmos. Chem., 61, 175–202, 2009.

Bond, T. C., Anderson, T. L., and Campbell, D.: Calibration and intercomparison of filter-based measurements of visible light absorption by aerosols, Aerosol Sci. Tech., 30, 582–600, 1999.

Bond, T. C., Streets, D. G., Yarber, K. F., Nelson, S. M., Woo, J.-H., and Klimont, Z.: A technology-based global inventory of black and organic carbon emissions from combustion, J. Geophys. Res., 109, D14203, 2004.

Bond, T. C., Doherty, S. J., Fahey, D. W., Forster, P. M., Berntsen, T., DeAngelo, B. J., Flanner, M. G., Ghan, S., Kärcher, B., Koch, D., Kinne, S., Kondo, Y., Quinn, P. K., Sarofim, M. C., Schultz, M. G., Schulz, M., Venkataraman, C., Zhang, H., Zhang, S., Bellouin, N., Guttikunda, S. K., Hopke, P. K., Jacobson, M. Z., Kaiser, J. W., Klimont, Z., Lohmann, U., Schwarz, J. P., Shindell, D., Storelvmo, T., Warren, S. G., and Zender, C. S.: Bounding the role of black carbon in the climate system: a scientific assessment, J. Geophys. Res.-Atmos., 118, 1–173, 2013.

Bressi, M., Sciare, J., Ghersi, V., Bonnaire, N., Nicolas, J. B., Petit, J.-E., Moukhtar, S., Rosso, A., Mihalopoulos, N., and Féron, A.: A one-year comprehensive chemical characterisation of fine aerosol ($PM_{2.5}$) at urban, suburban and rural background sites in the region of Paris (France), Atmos. Chem. Phys., 13, 7825–7844, doi:10.5194/acp-13-7825-2013, 2013.

Cappa, C. D., Onasch, T. B., Massoli, P., Worsnop, D. R., Bates, T. S., Cross, E. S., Davidovits, P., Hakala, J., Hayden, K. L., Jobson, B. T., Kolesar, K. R., Lack, D. A., Lerner, B. M., Li, S.-M., Mellon, D., Nuaaman, I., Olfert, J. S., Petäjä, T., Quinn, P. K., Song, C., Subramanian, R., Williams, E. J., and Zaveri, R. A.: Radiative absorption enhancements due to the mixing state of atmospheric black carbon, Science, 337, 1078–1081, 2012.

Chow, J. C., Watson, J. G., Lowenthal, D. H., Antony Chen, L.-W., and Motallebi, N.: $PM_{2.5}$ source profiles for black and organic carbon emission inventories, Atmos. Environ., 45, 5407–5414, 2011.

Dallmann, T. R. and Harley, R. A.: Evaluation of mobile source emission trends in the United States, J. Geophys. Res., 115, D14305, 2010.

Deguillaume, L., Beekmann, M., and Menut, L.: Bayesian Monte Carlo analysis applied to regional-scale inverse emission modeling for reactive trace gases, J. Geophys. Res., 112, D02307, 2007.

ACPD
14, 29237–29304, 2014

Denier van der Gon, H. A. C., Visschedijk, A., van der Brugh, H., and Dröge, R.: A high resolution European emission data base for the year 2005. A contribution to UBA-Projekt PAREST: Particle Reduction, Strategies, TNO-034-UT-2010-01895_RPT-ML, 2010.

Denier van der Gon, H. A. C., Beevers, S., D'Allura, A., Finardi, S., Honoré, C., Kuenen, J., Perrussel, O., Radice, P., Theloke, J., Uzbasich, M., and Visschedijk, A. : Discrepancies between top-down and bottom-up emission inventories of megacities: the causes and relevance for modeling concentrations and exposure, in: NATO Science for Peace and Security Series C: Environmental Security, edited by: Steyn, D. G. and Castelli, S. T., Vol. 4, 2011.

Dudhia, J.: A nonhydrostatic version of the Penn State-NCAR Mesoscale Model: validation tests and simulation of an Atlantic cyclone and cold front, Mon. Weather Rev., 121, 1493–1513, 1993.

Dunlea, E. J., Herndon, S. C., Nelson, D. D., Volkamer, R. M., San Martini, F., Sheehy, P. M., Zahniser, M. S., Shorter, J. H., Wormhoudt, J. C., Lamb, B. K., Allwine, E. J., Gaffney, J. S., Marley, N. A., Grutter, M., Marquez, C., Blanco, S., Cardenas, B., Retama, A., Ramos Villegas, C. R., Kolb, C. E., Molina, L. T., and Molina, M. J.: Evaluation of nitrogen dioxide chemiluminescence monitors in a polluted urban environment, Atmos. Chem. Phys., 7, 2691–2704, doi:10.5194/acp-7-2691-2007, 2007.

Folberth, G. A., Hauglustaine, D. A., Lathière, J., and Brocheton, F.: Interactive chemistry in the Laboratoire de Météorologie Dynamique general circulation model: model description and impact analysis of biogenic hydrocarbons on tropospheric chemistry, Atmos. Chem. Phys., 6, 2273–2319, doi:10.5194/acp-6-2273-2006, 2006.

Franco, V., Kousoulidou, M., Muntean, M., Ntziachristos, L., Hausberger, S., and Dilara, P.: Road vehicle emission factors development: a review, Atmos. Environ., 70, 84–97, 2013.

Freney, E. J., Sellegri, K., Canonaco, F., Colomb, A., Borbon, A., Michoud, V., Doussin, J.-F., Crumeyrolle, S., Amarouche, N., Pichon, J.-M., Bourianne, T., Gomes, L., Prevot, A. S. H., Beekmann, M., and Schwarzenböeck, A.: Characterizing the impact of urban emissions on regional aerosol particles: airborne measurements during the MEGAPOLI experiment, Atmos. Chem. Phys., 14, 1397–1412, doi:10.5194/acp-14-1397-2014, 2014.

Gilliland, A. and Abbitt, P. J.: A sensitivity study of the discrete Kalman filter (DKF) to initial condition discrepancies, J. Geophys. Res., 106, 17939, 2001.

Granier, C., Bessagnet, B., Bond, T., D'Angiola, A., Denier van der Gon, H. A. C., Frost, G. J., Heil, A., Kaiser, J. W., Kinne, S., Klimont, Z., Kloster, S., Lamarque, J.-F., Liousse, C., Masui, T., Meleux, F., Mieville, A., Ohara, T., Raut, J.-C., Riahi, K., Schultz, M. G., Smith, S. J.,

ACPD
14, 29237–29304, 2014

Thompson, A., Aardenne, J., Werf, G. R., and Vuuren, D. P.: Evolution of anthropogenic and biomass burning emissions of air pollutants at global and regional scales during the 1980–2010 period, Climatic Change, 109, 163–190, 2011.

Guenther, A., Karl, T., Harley, P., Wiedinmyer, C., Palmer, P. I., and Geron, C.: Estimates of global terrestrial isoprene emissions using MEGAN (Model of Emissions of Gases and Aerosols from Nature), Atmos. Chem. Phys., 6, 3181–3210, doi:10.5194/acp-6-3181-2006, 2006.

Haeffelin, M., Angelini, F., Morille, Y., Martucci, G., Frey, S., Gobbi, G. P., Lolli, S., O'Dowd, C. D., Sauvage, L., Xueref-Rémy, I., Wastine, B., and Feist, D. G.: Evaluation of mixing-height retrievals from automatic profiling lidars and ceilometers in view of future integrated networks in Europe, Bound.-Lay. Meteorol., 143, 49–75, 2012.

Hakami, A., Henze, D. K., Seinfeld, J. H., Chai, T., Tang, Y., Carmichael, G. R., and Sandu, A.: Adjoint inverse modeling of black carbon during the Asian Pacific Regional Aerosol Characterization Experiment, J. Geophys. Res., 110, D14301, 2005.

Hanna, S. R., Lu, Z., Christopher Frey, H., Wheeler, N., Vukovich, J., Arunachalam, S., Fernau, M., and Alan Hansen, D.: Uncertainties in predicted ozone concentrations due to input uncertainties for the UAM-V photochemical grid model applied to the July 1995 OTAG domain, Atmos. Environ., 35, 891–903, 2001.

Hansen, M. C. and Reed, B.: A comparison of the IGBP DISCover and University of Maryland 1 km global land cover products, Int. J. Remote Sens., 21, 1365–1373, 2000.

Hansen, M. C., Defries, R. S., Townshend, J. R. G., and Sohlberg, R.: Global land cover classification at 1 km spatial resolution using a classification tree approach, Int. J. Remote Sens., 21, 1331–1364, 2000.

Hauglustaine, D. A., Hourdin, F., Jourdain, L., Filiberti, M.-A., Walters, S., Lamarque, J.-F., and Holland, E. A.: Interactive chemistry in the Laboratoire de Meteorology Dyanmique general circulation model: description and background tropospheric chemistry evaluation, J. Geophys. Res., 109, D04314, 2004.

Healy, R. M., Sciare, J., Poulain, L., Kamili, K., Merkel, M., Müller, T., Wiedensohler, A., Eckhardt, S., Stohl, A., Sarda-Estève, R., McGillicuddy, E., O'Connor, I. P., Sodeau, J. R., and Wenger, J. C.: Sources and mixing state of size-resolved elemental carbon particles in a European megacity: Paris, Atmos. Chem. Phys., 12, 1681–1700, doi:10.5194/acp-12-1681-2012, 2012.

ACPD
14, 29237–29304, 2014

Junker, C. and Liousse, C.: A global emission inventory of carbonaceous aerosol from historic records of fossil fuel and biofuel consumption for the period 1860–1997, Atmos. Chem. Phys., 8, 1195–1207, doi:10.5194/acp-8-1195-2008, 2008.
Konovalov, I. B., Beekmann, M., Richter, A., and Burrows, J. P.: Inverse modelling of the spatial distribution of NO_x emissions on a continental scale using satellite data, Atmos. Chem. Phys., 6, 1747–1770, doi:10.5194/acp-6-1747-2006, 2006.
Konovalov, I. B., Beekmann, M., Burrows, J. P., and Richter, A.: Satellite measurement based estimates of decadal changes in European nitrogen oxides emissions, Atmos. Chem. Phys., 8, 2623–2641, doi:10.5194/acp-8-2623-2008, 2008.
Lamarque, J.-F., Bond, T. C., Eyring, V., Granier, C., Heil, A., Klimont, Z., Lee, D., Liousse, C., Mieville, A., Owen, B., Schultz, M. G., Shindell, D., Smith, S. J., Stehfest, E., Van Aardenne, J., Cooper, O. R., Kainuma, M., Mahowald, N., McConnell, J. R., Naik, V., Riahi, K., and van Vuuren, D. P.: Historical (1850–2000) gridded anthropogenic and biomass burning emissions of reactive gases and aerosols: methodology and application, Atmos. Chem. Phys., 10, 7017–7039, doi:10.5194/acp-10-7017-2010, 2010.
Liousse, C., Cachier, H., and Jennings, S. G.: Optical and thermal measurements of black carbon aerosol content in different environments: variation of the specific attenuation cross-section, sigma (σ), Atmos. Environ. A-Gen., 27, 1203–1211, 1993.
Lohmann, U. and Feichter, J.: Global indirect aerosol effects: a review, Atmos. Chem. Phys., 5, 715–737, doi:10.5194/acp-5-715-2005, 2005.
McNaughton, C. S., Clarke, A. D., Howell, S. G., Pinkerton, M., Anderson, B., Thornhill, L., Hudgins, C., Winstead, E., Dibb, J. E., Scheuer, E., and Maring, H.: Results from the DC-8 Inlet Characterization Experiment (DICE): airborne versus surface sampling of mineral dust and sea salt aerosols, Aerosol Sci. Tech., 41, 136–159, 2007.
Mendoza-Dominguez, A. and Russell, A. G.: Iterative inverse modeling and direct sensitivity analysis of a photochemical air quality model, Environ. Sci. Technol., 34, 4974–4981, 2000.
Menut, L., Bessagnet, B., Khvorostyanov, D., Beekmann, M., Blond, N., Colette, A., Coll, I., Curci, G., Foret, G., Hodzic, A., Mailler, S., Meleux, F., Monge, J.-L., Pison, I., Siour, G., Turquety, S., Valari, M., Vautard, R., and Vivanco, M. G.: CHIMERE 2013: a model for regional atmospheric composition modelling, Geosci. Model Dev., 6, 981–1028, doi:10.5194/gmd-6-981-2013, 2013.
Napelenok, S. L., Pinder, R. W., Gilliland, A. B., and Martin, R. V.: A method for evaluating spatially-resolved NO_x emissions using Kalman filter inversion, direct sensitivities, and

ACPD
14, 29237–29304, 2014

space-based NO_2 observations, Atmos. Chem. Phys., 8, 5603–5614, doi:10.5194/acp-8-5603-2008, 2008.
Napelenok, S. L., Foley, K. M., Kang, D., Mathur, R., Pierce, T., and Rao, S. T.: Dynamic evaluation of regional air quality model's response to emission reductions in the presence of uncertain emission inventories, Atmos. Environ., 45, 4091–4098, 2011.
Nenes, A., Pandis, S., and Pilinis, C.: ISORROPIA: a new thermodynamic equilibrium model for multiphase multicomponent inorganic aerosols, Aquat. Geochem., 123–152, 1998.
Parrish, D. D.: Critical evaluation of US on-road vehicle emission inventories, Atmos. Environ., 40, 2288–2300, 2006.
Peng, R. D., Bell, M. L., Geyh, A. S., McDermott, A., Zeger, S. L., Samet, J. M., and Dominici, F.: Emergency admissions for cardiovascular and respiratory diseases and the chemical composition of fine particle air pollution., Environ. Health Persp., 117, 957–63, 2009.
Petetin, H., Beekmann, M., Sciare, J., Bressi, M., Rosso, A., Sanchez, O., and Ghersi, V.: A novel model evaluation approach focusing on local and advected contributions to urban $PM_{2.5}$ levels – application to Paris, France, Geosci. Model Dev., 7, 1483–1505, doi:10.5194/gmd-7-1483-2014, 2014.
Petzold, A., Ogren, J. A., Fiebig, M., Laj, P., Li, S.-M., Baltensperger, U., Holzer-Popp, T., Kinne, S., Pappalardo, G., Sugimoto, N., Wehrli, C., Wiedensohler, A., and Zhang, X.-Y.: Recommendations for reporting "black carbon" measurements, Atmos. Chem. Phys., 13, 8365–8379, doi:10.5194/acp-13-8365-2013, 2013.
Pouliot, G., Pierce, T. E., Denier van der Gon, H., Schaap, M., Moran, M., and Nopmongeol, U.: Comparing emission inventories and model-ready emission datasets between Europe and North America for the AQMEII project, Atmos. Environ., 53, 4–14, 2012.
Schmidt, H. and Derognat, C.: A comparison of simulated and observed ozone mixing ratios for the summer of 1998 in Western Europe, Atmos. Environ., 35, 6277–6297, 2001.
Schulz, M., Textor, C., Kinne, S., Balkanski, Y., Bauer, S., Berntsen, T., Berglen, T., Boucher, O., Dentener, F., Guibert, S., Isaksen, I. S. A., Iversen, T., Koch, D., Kirkevåg, A., Liu, X., Montanaro, V., Myhre, G., Penner, J. E., Pitari, G., Reddy, S., Seland, Ø., Stier, P., and Takemura, T.: Radiative forcing by aerosols as derived from the AeroCom present-day and pre-industrial simulations, Atmos. Chem. Phys., 6, 5225–5246, doi:10.5194/acp-6-5225-2006, 2006.
Sciare, J., d'Argouges, O., Sarda-Estève, R., Gaimoz, C., Dolgorouky, C., Bonnaire, N., Favez, O., Bonsang, B., and Gros, V.: Large contribution of water-insoluble secondary or-

ACPD
14, 29237–29304, 2014

ganic aerosols in the region of Paris (France) during wintertime, J. Geophys. Res., 116, D22203, 2011.
Skamarock, W. C., Klemp, J. B., Gill, D. O., Barker, D. M., and Powers, J. G.: A description of the advanced research WRF Version 2, Tech. Rep., 2005.
Smit, R., Ntziachristos, L., and Boulter, P.: Validation of road vehicle and traffic emission models – a review and meta-analysis, Atmos. Environ., 44, 2943–2953, 2010.
Tian, D., Cohan, D. S., Napelenok, S., Bergin, M., Hu, Y., Chang, M., and Russell, A. G.: Uncertainty analysis of ozone formation and response to emission controls using higher-order sensitivities, J. Air Waste Manage., 60, 797–804, 2010.
Timmermans, R., Denier van der Gon, H. A. C., Kuenen, J. J. P., Segers, A. J., Honoré, C., Perrussel, O., Builtjes, P. J. H., and Schaap, M.: Quantification of the urban air pollution increment and its dependency on the use of down-scaled and bottom-up city emission inventories, Urban Climate, 6, 44–62, 2013.
Troen, I. B. and Mahrt, L.: A simple model of the atmospheric boundary layer; sensitivity to surface evaporation, Bound.-Lay. Meteorol., 37, 129–148, 1986.
Vautard, R., Martin, D., Beekmann, M., Drobinski, P., Friedrich, R., Jaubertie, A., Kley, D., Lattuati, M., Moral, P., Neininger, B., and Theloke, J.: Paris emission inventory diagnostics from ESQUIF airborne measurements and a chemistry transport model, J. Geophys. Res., 108, 8564, 2003.
Vestreng, V., Mareckova, K., Kakareka, S., Malchykhina, A., and Kukharchyk, T.: Inventory Review 2007 – Emission data reported to LRTAP Convention and NEC Directive, Tech. rep., 2007.
Vignati, E., Karl, M., Krol, M., Wilson, J., Stier, P., and Cavalli, F.: Sources of uncertainties in modelling black carbon at the global scale, Atmos. Chem. Phys., 10, 2595–2611, doi:10.5194/acp-10-2595-2010, 2010.
Virkkula, A., Ahlquist, N. C., Covert, D. S., Arnott, W. P., Sheridan, P. J., Quinn, P. K., and Coffman, D. J.: Modification, calibration and a field test of an instrument for measuring light absorption by particles, Aerosol Sci. Tech., 39, 68–83, 2005.
Xu, W., Zhao, C., Ran, L., Deng, Z., Ma, N., Liu, P., Lin, W., Yan, P., and Xu, X.: A new approach to estimate pollutant emissions based on tra jectory modeling and its application in the North China Plain, Atmos. Environ., 71, 75–83, 2013.
Yu, H., Kaufman, Y. J., Chin, M., Feingold, G., Remer, L. A., Anderson, T. L., Balkanski, Y., Bellouin, N., Boucher, O., Christopher, S., DeCola, P., Kahn, R., Koch, D., Loeb, N., Reddy, M. S.,

ACPD
14, 29237–29304, 2014

Schulz, M., Takemura, T., and Zhou, M.: A review of measurement-based assessments of the aerosol direct radiative effect and forcing, Atmos. Chem. Phys., 6, 613–666, doi:10.5194/acp-6-613-2006, 2006.

Zhang, Q. J., Beekmann, M., Drewnick, F., Freutel, F., Schneider, J., Crippa, M., Prevot, A. S. H., Baltensperger, U., Poulain, L., Wiedensohler, A., Sciare, J., Gros, V., Borbon, A., Colomb, A., Michoud, V., Doussin, J.-F., Denier van der Gon, H. A. C., Haeffelin, M., Dupont, J.-C., Siour, G., Petetin, H., Bessagnet, B., Pandis, S. N., Hodzic, A., Sanchez, O., Honoré, C., and Perrussel, O.: Formation of organic aerosol in the Paris region during the MEGAPOLI summer campaign: evaluation of the volatility-basis-set approach within the CHIMERE model, Atmos. Chem. Phys., 13, 5767–5790, doi:10.5194/acp-13-5767-2013, 2013.

Zhou, X., Gao, J., Wang, T., Wu, W., and Wang, W.: Measurement of black carbon aerosols near two Chinese megacities and the implications for improving emission inventories, Atmos. Environ., 43, 3918–3924, 2009.

ACPD
14, 29237–29304, 2014

Table 1. Description of domains.

Domain name	Cells number (SW corner location)	Resolution
CONT3	67 × 46 (−10.5; 35)	0.5° × 0.5° (~ 50 km × 50 km)
MEG3	120 × 120 (−0.35; 47.45)	0.04° × 0.027°

ACPD
14, 29237–29304, 2014

Table 2. Statistical results of MM5 (and WRF in parenthesis) considering all July hours and only the 06:00–14:00 UTC time window (*N* represents the proportion of available data).

Time range	Parameter	MB	NMB (%)	RMSE	NRMSE (%)	R (/)	*N* (%)
All hours	Temperature (°C)	−0.87 (+0.45)	–	1.94 (1.57)	–	0.92 (0.94)	90
	Wind speed ($m s^{-1}$)	+0.83 (+0.99)	+33 (+39)	1.35 (1.47)	53 (58)	0.78 (0.80)	90
	BLH (m)	−440 (−224)	−34 (−17)	769 (553)	59 (43)	0.50 (0.69)	76
06:00–14:00 UTC	Temperature (°C)	−0.45 (+0.29)	–	1.76 (1.60)	–	0.92 (0.94)	89
	Wind speed ($m s^{-1}$)	+1.04 (+0.71)	+35 (+24)	1.46 (1.18)	49 (39)	0.79 (0.84)	89
	BLH (m)	−345 (−176)	−24 (−12)	657 (530)	46 (37)	0.52 (0.65)	88

ACPD
14, 29237–29304, 2014

Table 3. Wind speed statistical results during flight days, between 06:00–14:00 UTC, in the altitude range of 110–210 m, for MM5 model (and WRF in parenthesis).

July day	Mean observation ($m\,s^{-1}$)	NMB (%)	NRMSE (%)
9	7.03	+3.2 (+3.1)	23 (13)
10	6.36	+1.9 (+9.0)	12 (18)
13	5.08	−21 (−34)	25 (36)
15	9.14	+0.51 (−6.1)	12 (9.4)
16	3.69	−34 (−39)	44 (47)
21	7.55	+12 (+2.7)	32 (26)
25	6.31	+5.3 (−3.2)	12 (11)
28	3.83	−17 (−46)	31 (58)
29	4.42	+27 (+8.8)	29 (19)
All	5.93	−0.27 (−8.0)	24 (25)

ACPD
14, 29237–29304, 2014

Table 4. Statistical results on BC ($\mu g\,m^{-3}$), NO_x (ppb) and BC/NO_x ratio ($\mu g\,m^{-3}\,ppb^{-1}$) at the LHVP site.

Species	Case	MB	NMB (%)	RMSE	NRMSE (%)	R	N (%)
BC	EMEP (MM5)	+1.1	+93	2.0	170	0.42	99
	TNO (MM5)	+3.1	+260	4.5	372	0.39	99
	TNO-MP (MM5)	+1.3	+110	2.3	191	0.43	99
	EMEP (WRF)	+0.5	+43	1.3	106	0.70	99
	TNO (WRF)	+2.2	+187	3.7	312	0.67	99
	TNO-MP (WRF)	+0.7	+59	1.6	135	0.70	99
NO_x	EMEP (MM5)	+1.0	+5	23.6	108	0.40	96
	TNO (MM5)	+7.8	+36	26.8	122	0.40	96
	TNO-MP (MM5)	+12.8	+58	30.8	141	0.38	96
	EMEP (WRF)	−5.4	−25	15.7	72	0.77	96
	TNO (WRF)	+0.8	+4	17.2	78	0.72	96
	TNO-MP (WRF)	+4.8	+22	19.8	90	0.71	96
BC/NO_x	EMEP (MM5)	+0.04	+67	0.05	87	0.22	95
	TNO (MM5)	+0.08	+131	0.09	146	−0.15	95
	TNO-MP (MM5)	+0.01	+13	0.03	56	0.17	95
	EMEP (WRF)	+0.04	+72	0.06	90	0.23	95
	TNO (WRF)	+0.08	+136	0.09	150	−0.07	95
	TNO-MP (WRF)	+0.01	+11	0.03	55	0.19	95

ACPD
14, 29237–29304, 2014

Table 5. BC vs. NO_x slopes and emission error factors over the 05:00–8:00 UTC time window.

Case		Flight dates BC vs. NO_x ($\mu g\,m^{-3}\,ppb^{-1}$)	Model/observations ratio [uncertainty*]	All July dates BC vs. NO_x ($\mu g\,m^{-3}\,ppb^{-1}$)	Model/observations ratio [uncertainty*]
MM5	EMEP	0.093 ± 0.003	2.82 [18 %]	0.095 ± 0.001	2.79 [11 %]
	TNO	0.135 ± 0.009	4.09 [19 %]	0.128 ± 0.005	3.76 [11 %]
	TNO-MP	0.075 ± 0.002	2.27 [18 %]	0.074 ± 0.001	2.18 [11 %]
WRF	EMEP	0.097 ± 0.002	2.94 [18 %]	0.097 ± 0.001	2.85 [11 %]
	TNO	0.154 ± 0.010	4.67 [19 %]	0.140 ± 0.006	4.12 [11 %]
	TNO-MP	0.073 ± 0.002	2.21 [18 %]	0.072 ± 0.001	2.12 [11 %]
Observations		0.033 ± 0.006	–	0.034 ± 0.004	–

* At a 95 % confidence interval.

ACPD
14, 29237–29304, 2014

Table 6. BC/NO_x mean results.

Meteorological data	Inventory	Mean bias	Uncertainty factor	Confidence interval
MM5	EMEP	−18 %	1.41	(−42 %; +16 %)
	TNO	+7 %	1.41	(−24 %; +50 %)
	TNO-MP	−46 %	1.34	(−60 %; −28 %)
WRF	EMEP	−18 %	1.36	(−40 %; +12 %)
	TNO	+13 %	1.36	(−17 %; +53 %)
	TNO-MP	−44 %	1.31	(−57 %; −26 %)

ACPD
14, 29237–29304, 2014

Table 7. Systematic two-sigma uncertainties on BC and NO_x error factors and BC/NO_x error factor ratio from various sources, and associated confidence intervals on average emission error biases for the three inventories.

Uncertainty source	BC	NO_x	BC/NO_x
Boundary layer height	14 %	14 %	1 %
Vertical mixing	17 %	19 %	6 %
Deposition	7 %	16 %	9 %
Mass-specific absorption coefficient	30 %	–	30 %
NO_x and absorption coefficient measurement	30 %	20 %	36 %
Overall uncertainty	48 %	35 %	48 %

ACPD
14, 29237–29304, 2014

Table 8. Confidence intervals on average emission error biases for the three inventories.

Inventory	BC	NO_x	BC/NO_x
EMEP	+12 % (−24 %; +66 %)	+29 % (−4 %; +74 %)	−18 % (−45 %; +22 %)
TNO	+40 % (−6 %; +108 %)	+18 % (−12 %; +59 %)	+13 % (−24 %; +67 %)
TNO-MP	−23 % (−48 %; +15 %)	+29 % (−4 %; +74 %)	−44 % (−62 %; −17 %)

ACPD
14, 29237–29304, 2014

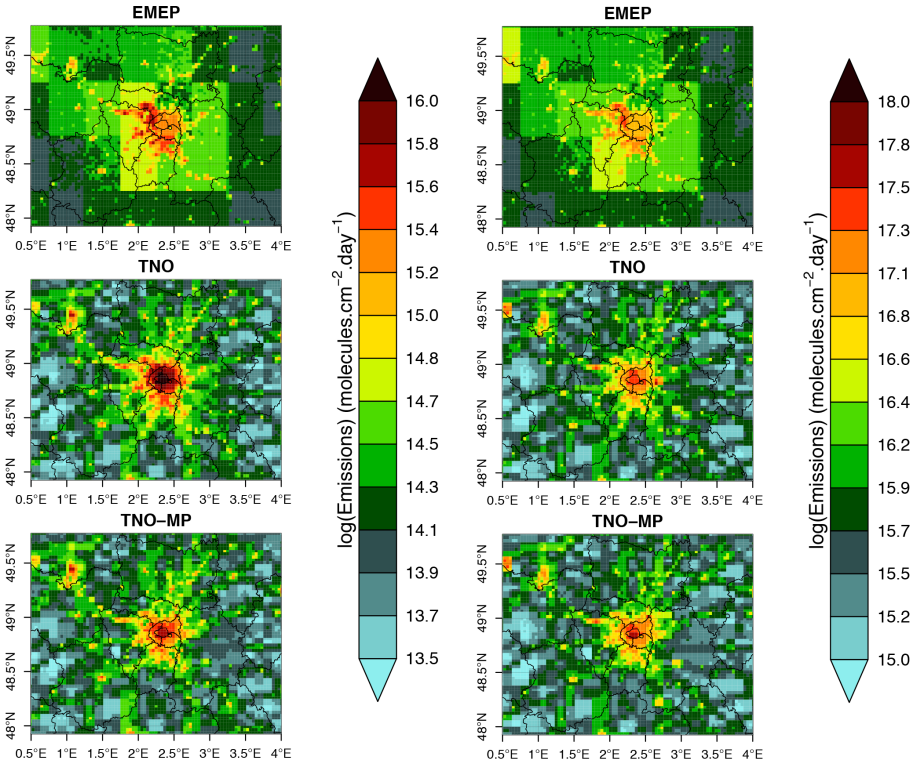

Figure 1. BC (left panel) and NO_x (right panel) emissions in EMEP, TNO and TNO-MP inventories.

ACPD
14, 29237–29304, 2014

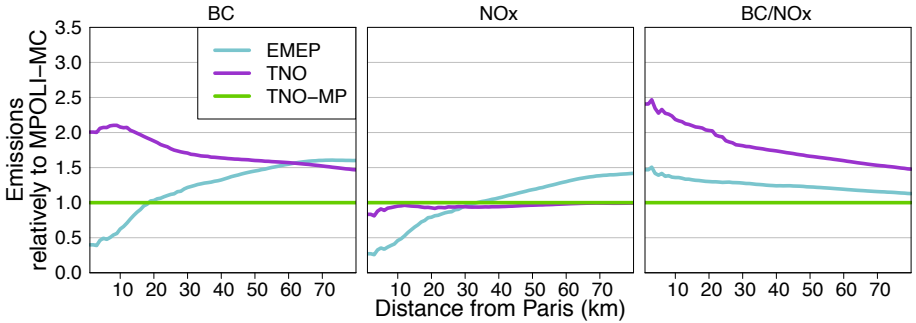

Figure 2. Integrated BC, NO_x and BC/NO_x emissions at various distances from the LHVP site, relatively to the TNO-MP inventory.

ACPD
14, 29237–29304, 2014

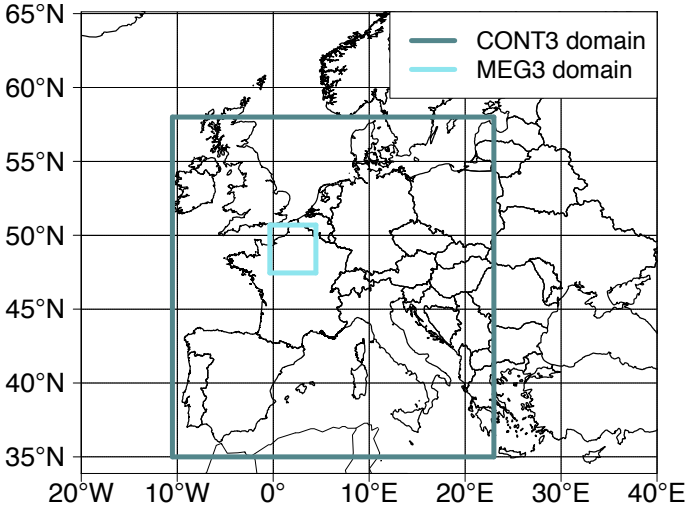

Figure 3. Nested domains.

ACPD
14, 29237–29304, 2014

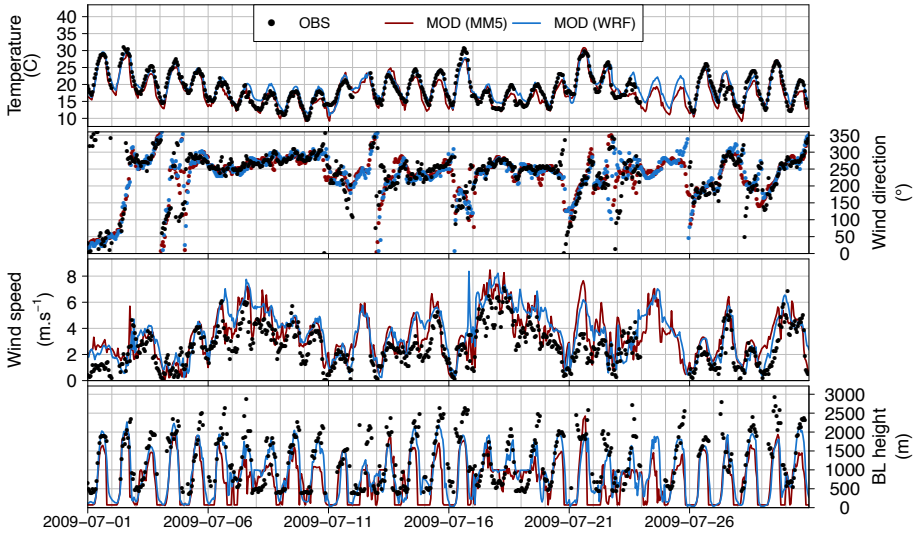

Figure 4. Wind (at 10 m), temperature (at 2 m) and BLH time series in July 2009 at SIRTA site.

ACPD
14, 29237–29304, 2014

Evaluating BC and NO_x emission inventories

H. Petetin et al.

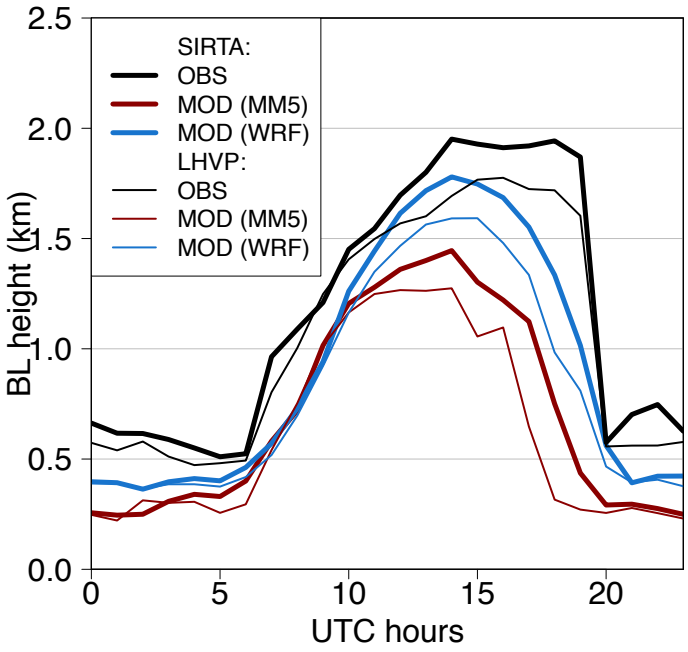

Figure 5. Observed and simulated diurnal profile of BLH at SIRTA and LHVP sites.

ACPD
14, 29237–29304, 2014

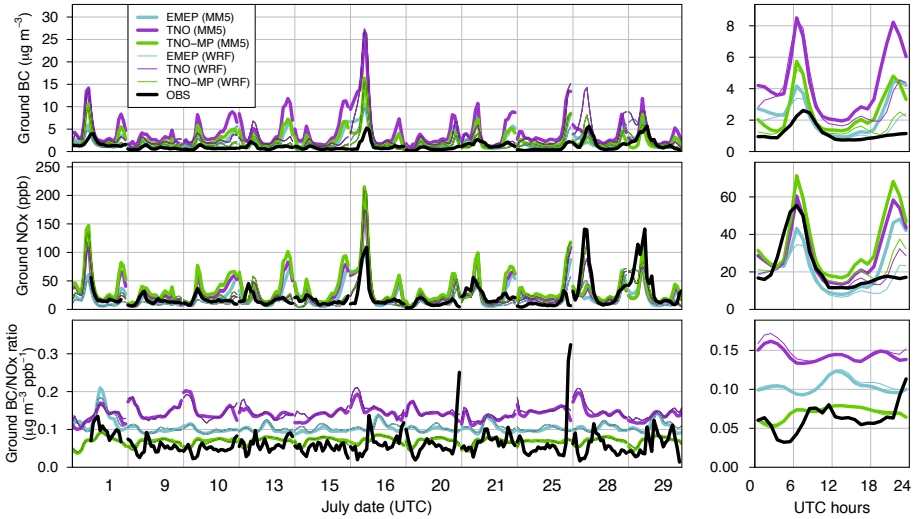

Figure 6. BC, NO_x and BC/NO_x ratio concentration at LHVP urban background site during July flight dates (left panel) and associated diurnal profiles (right panel).

ACPD
14, 29237–29304, 2014

Evaluating BC and NO_x emission inventories

H. Petetin et al.

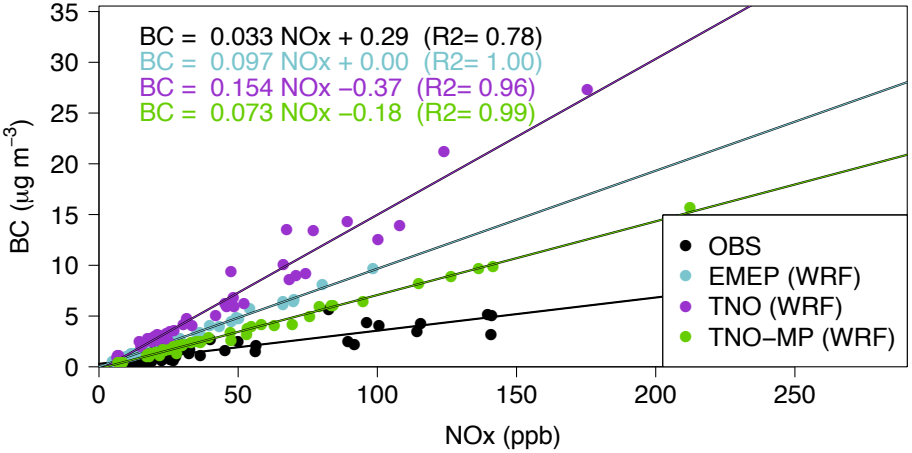

Figure 7. Observed and simulated BC vs. NO_x concentrations at LHVP between 05:00–8:00 UTC considering July flight days, and linear fits (lines). Only simulations with WRF meteorological data are reported here.

ACPD
14, 29237–29304, 2014

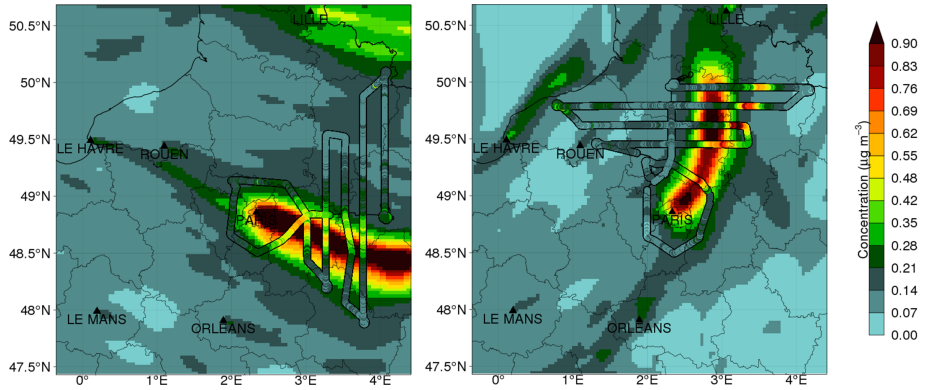

Figure 8. Observed (along the aircraft trajectory) and modeled (in background, with the TNO-MM5 case) BC concentration for 10 July (left panel) and 13 (right panel). Paris and some other large cities are indicated. Simulated concentrations shown here are taken at 13:00 UTC on the 4th layer that roughly corresponds to 470–870 m height. The solid black line corresponds to the flight path outside that layer (altitude above 870 m or below 470 m).

ACPD
14, 29237–29304, 2014

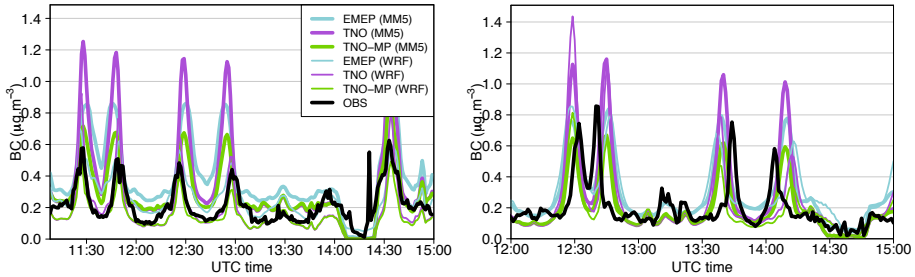

Figure 9. Observed (in black) and simulated BC concentrations along the aircraft trajectory for 10 July (left panel) and 13 (right panel).

ACPD
14, 29237–29304, 2014

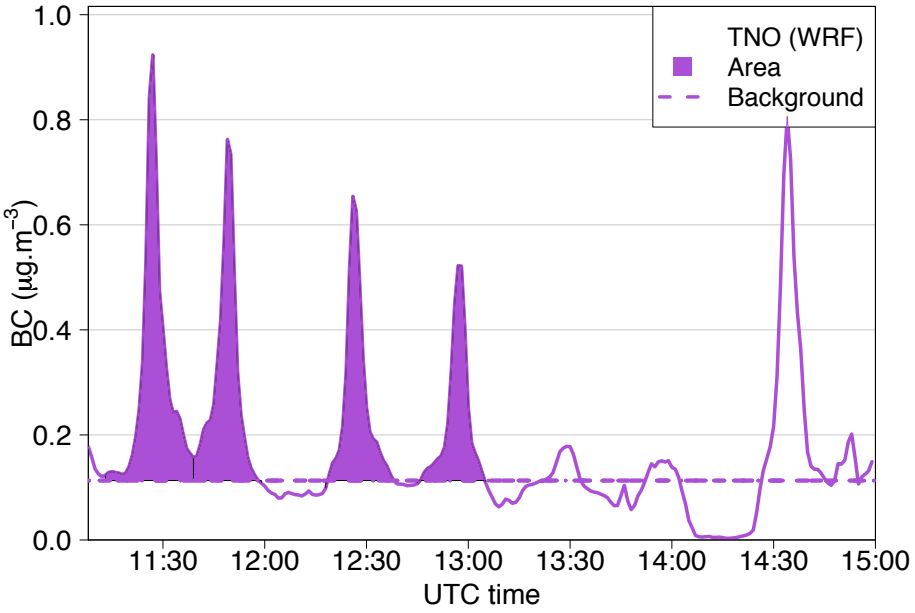

Figure 10. Peak integral (purple area) above background (dotted line) for the TNO/WRF simulation the 10 July.

ACPD
14, 29237–29304, 2014

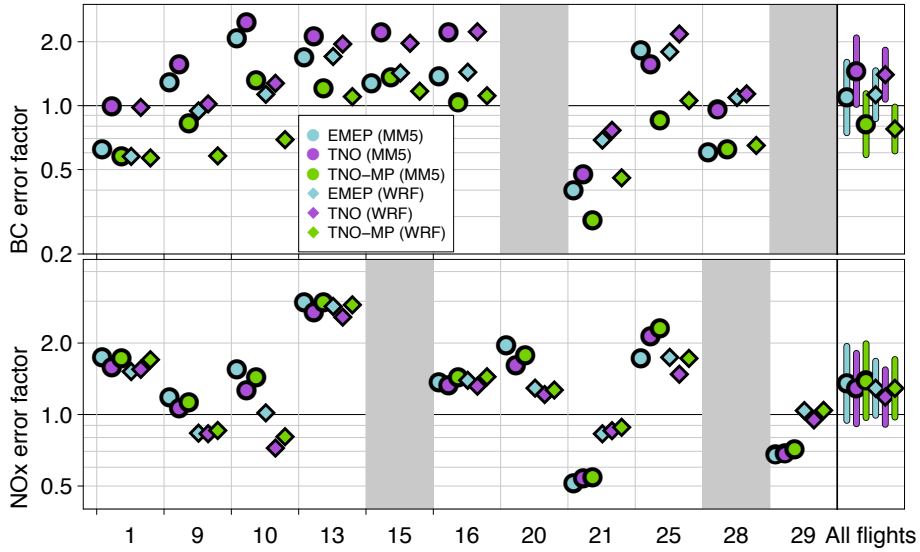

Figure 11. BC (top panel) and NO_x (bottom panel) emission error factors for each individual flight (when available) and averaged emission error factor (on the top right) with 95 % confidence interval, for all six simulated cases (logarithmic scale).

ACPD
14, 29237–29304, 2014

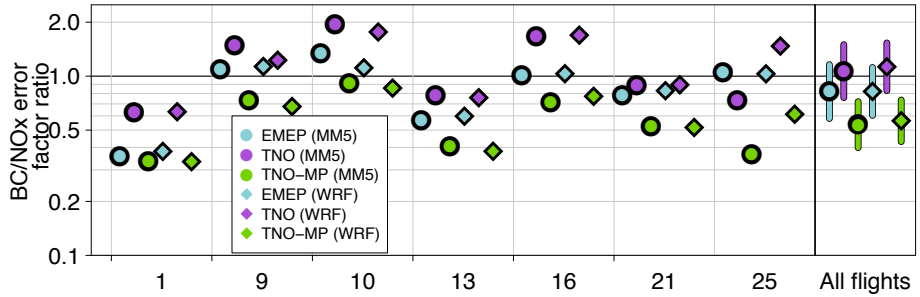

Figure 12. BC/NO_x emission error factors ratio for each individual flight and averaged for all flights (on the right) with confidence interval, for all six simulated cases (logarithmic scale).

ACPD
14, 29237–29304, 2014

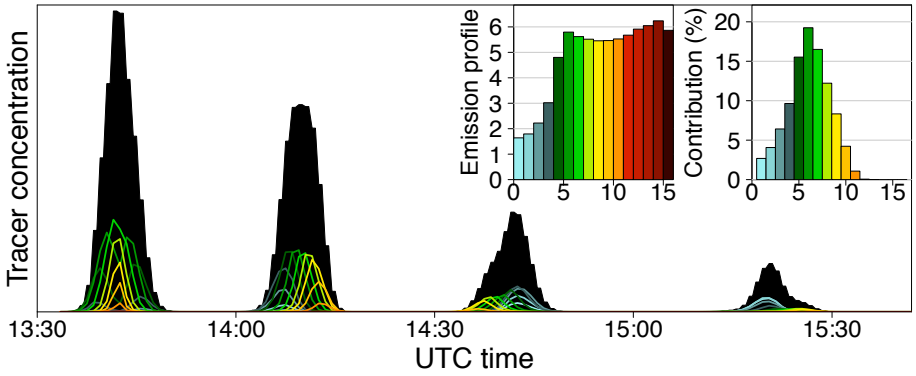

Figure 13. Concentration along the flight trajectory of the 16 tracers (in color line) and their total (in black) during the 28 July flight. The emission profile gives the color associated to each tracer as well as their emission intensity. The contribution over all peaks of each tracer to the total (in terms of area) is shown in the top right corner.

ACPD
14, 29237–29304, 2014

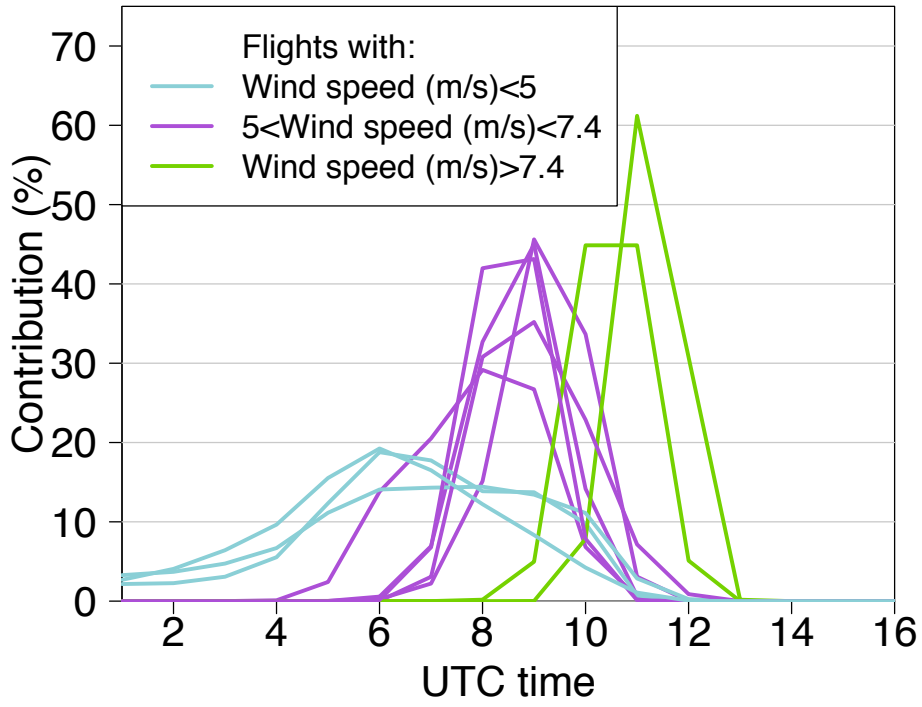

Figure 14. Hourly emissions contribution to total area for all flights. At each flight corresponds a line colored according to the mean wind speed given in Table 3 (see Sect. 4.1.2). Note that, as flights occur in the afternoon, only the 16 first hours of the day are represented.

ACPD
14, 29237–29304, 2014

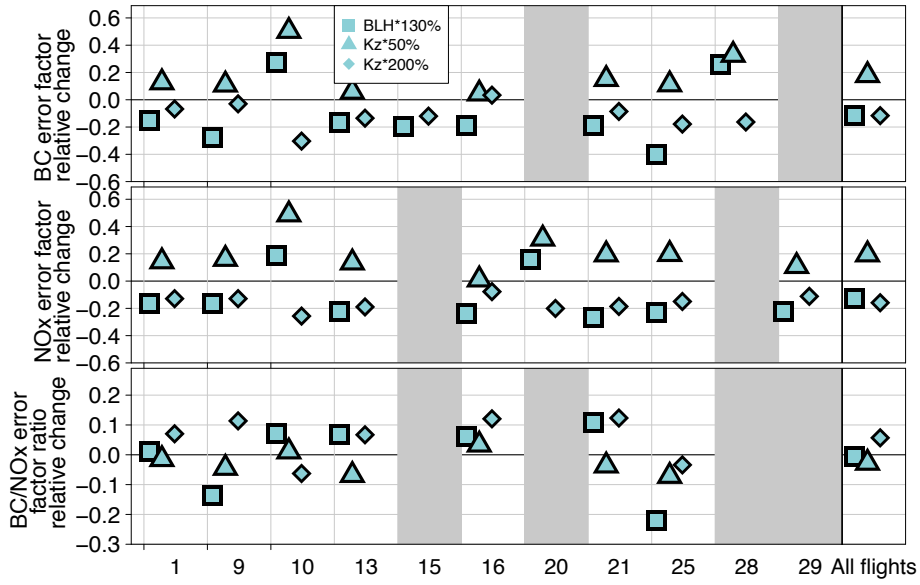

Figure 15. BC and NO_x emission error factors relative changes with modified K_z and BLH (and EMEP/TNO-MP taken as reference) for MM5 meteorology.

ACPD
14, 29237–29304, 2014